

1 Importance of Dry Deposition Parameterization Choice in Global 2 Simulations of Surface Ozone

3 Anthony Y.H. Wong¹, Jeffrey A. Geddes¹, Amos P.K. Tai^{2,3}, Sam J. Silva⁴

4 ¹Department of Earth and Environment, Boston University, Boston, MA, USA

5 ²Earth System Science Programme, Faculty of Science, The Chinese University of Hong Kong, Hong Kong

6 ³Institute of Energy, Environment and Sustainability, and State Key Laboratory of Agrobiotechnology, The Chinese University
7 of Hong Kong, Hong Kong

8 ⁴Department of Civil and Environmental Engineering, Massachusetts Institute of Technology, Cambridge, MA, USA

9 *Correspondence to:* Jeffrey A. Geddes (jgeddes@bu.edu)

10 **Abstract.** Dry deposition is a major sink of tropospheric ozone. Increasing evidence has shown that ozone dry deposition
11 actively links meteorology and hydrology with ozone air quality. However, there is little systematic investigation on the
12 performance of different ozone dry deposition parameterizations at the global scale, and how parameterization choice can
13 impact surface ozone simulations. Here we present the results of the first global, multi-decade modelling and evaluation of
14 ozone dry deposition velocity (v_d) using multiple ozone dry deposition parameterizations. We model ozone dry deposition
15 velocities over 1982-2011 using four ozone dry deposition parameterizations that are representative of current approaches in
16 global ozone dry deposition modelling. We use consistent assimilated meteorology, land cover, and satellite-derived leaf area
17 index (LAI) across all four, such that the differences in simulated v_d are entirely due to differences in deposition model
18 structures or assumptions about how land types are treated in each. In addition, we use the surface ozone sensitivity to v_d
19 predicted by a chemical transport model to estimate the impact of mean and variability of ozone dry deposition velocity on
20 surface ozone. Our estimated v_d from four different parameterizations are evaluated against field observations, and while
21 performance varies considerably by land cover types, our results suggest that none of the parameterizations are universally
22 better than the others. Discrepancy in simulated mean v_d among the parameterizations is estimated to cause 2 to 5 ppbv of
23 discrepancy in surface ozone in the Northern Hemisphere (NH) and up to 8 ppbv in tropical rainforests in July, and up to 8
24 ppbv in tropical rainforests and seasonally dry tropical forests in Indochina in December. Parameterization-specific biases
25 based on individual land cover type and hydroclimate are found to be the two main drivers of such discrepancies. We find
26 statistically significant trends in the multiannual time series of simulated July daytime v_d in all parameterizations, driven by
27 warming and drying (southern Amazonia, southern African savannah and Mongolia) or greening (high latitudes). The trend in
28 July daytime v_d is estimated to be 1 % yr⁻¹ and leads to up to 3 ppbv of surface ozone changes over 1982-2011. The interannual
29 coefficient of variation (CV) of July daytime mean v_d in NH is found to be 5%-15%, with spatial distribution that varies with
30 the dry deposition parameterization. Our sensitivity simulations suggest this can contribute between 0.5 to 2 ppbv to
31 interannual variability (IAV) in surface ozone, but all models tend to underestimate interannual CV when compared to long-
32 term ozone flux observations. We also find that IAV in some dry deposition parameterizations are more sensitive to LAI while

33 others are more sensitive to climate. Comparisons with other published estimates of the IAV of background ozone confirm
34 that ozone dry deposition can be an important part of natural surface ozone variability. Our results demonstrate the importance
35 of ozone dry deposition parameterization choice on surface ozone modelling, and the impact of IAV of v_d on surface ozone,
36 thus making a strong case for further measurement, evaluation and model-data integration of ozone dry deposition on different
37 spatiotemporal scales.

38 **1 Introduction**

39 Surface ozone (O_3) is one of the major air pollutants that poses serious threats to human health (Jerrett et al., 2009) and plant
40 productivity (Ainsworth et al., 2012; Reich, 1987; Wittig et al., 2007). Ozone exerts additional pressure on global food security
41 and public health by damaging agricultural ecosystems and reducing crop yields (Avnery et al., 2011; McGrath et al., 2015;
42 Tai et al., 2014). Dry deposition, by which atmospheric constituents are removed from the atmosphere and transferred to the
43 Earth's surface through turbulent transport or gravitational settling, is the second-largest and terminal sink of tropospheric O_3
44 (Wild, 2007). Terrestrial ecosystems are particularly efficient at removing O_3 via dry deposition through stomatal uptake and
45 other non-stomatal pathways (Wesely and Hicks, 2000) (e.g., cuticle, soil, reaction with biogenic volatile organic compounds
46 (BVOCs) (Fares et al., 2010; Wolfe et al., 2011). Meanwhile, stomatal uptake of O_3 inflicts damage on plants by initiating
47 reactions that impair their photosynthetic and stomatal regulatory capacity (Hoshika et al., 2014; Lombardozzi et al., 2012;
48 Reich, 1987). Widespread plant damage has the potential to alter the global water cycle (Lombardozzi et al., 2015) and suppress
49 the land carbon sink (Sitch et al., 2007), as well as to generate a cascade of feedbacks that affect atmospheric composition
50 including ozone itself (Sadiq et al., 2017; Zhou et al., 2018). Ozone dry deposition is therefore key in understanding how
51 meteorology (Kavassalis and Murphy, 2017), climate, and land cover change (Fu and Tai, 2015; Ganzeveld et al., 2010; Geddes
52 et al., 2016; Heald and Geddes, 2016; Sadiq et al., 2017; Sanderson et al., 2007; Young et al., 2013) can affect air quality and
53 atmospheric chemistry at large.

54

55 Analogous to other surface-atmosphere exchange processes (e.g., sensible and latent heat flux), O_3 dry deposition flux (F_{O_3})
56 is often expressed as the product of ambient O_3 concentrations at the surface ($[O_3]$) and a transfer coefficient (dry deposition
57 velocity, v_d) that describes the efficiency of transport (and removal) to the surface from the measurement height:

58

$$F_{O_3} = [O_3]v_d \quad (1)$$

59 Also analogous to other surface fluxes, F_{O_3} , $[O_3]$, and hence v_d can be directly measured by the eddy covariance (EC) method
60 (e.g. Fares et al., 2014; Gerosa et al., 2005; Lamaud et al., 2002; Munger et al., 1996; Rannik et al., 2012) with random
61 uncertainty of about 20% (Keronen et al., 2003; Muller et al., 2010). Apart from EC, F_{O_3} and v_d can also be estimated from
62 the vertical profile of O_3 by exploiting flux-gradient relationship (Foken, 2006) (termed the gradient method, GM) (e.g. Gerosa
63 et al., 2017; Wu et al., 2016, 2015). A recent study (Silva and Heald, 2018) compiled 75 sets of ozone deposition measurement
64 from the EC and GM across different seasons and land cover types over the past 30 years.

65

66 At the site level, ozone dry deposition over various terrestrial ecosystems can be simulated comprehensively by 1-D chemical
67 transport models (Ashworth et al., 2015; Wolfe et al., 2011; Zhou et al., 2017), which are able to simulate the effects of vertical
68 gradients inside the canopy environment, and gas-phase reaction with BVOCs in addition to surface sinks. Regional and global
69 models, which lack the fine-scale information (e.g. vertical structure of canopy, in-canopy BVOCs emissions) and horizontal
70 resolution for resolving the plant canopy in such detail, instead represent plant canopy foliage as 1 to 2 big leaves, and v_d is
71 parameterized as a network of resistances, which account for the effects of turbulent mixing via aerodynamic (R_a), molecular
72 diffusion via quasi-laminar sublayer resistances (R_b), and surface sinks via surface resistance (R_c):

73
$$v_d = \frac{1}{R_a + R_b + R_c} \quad (2)$$

74

75 A diverse set of parameterizations of ozone dry deposition are available and used in different models and monitoring networks.
76 Examples include the Wesely parameterization (1989) and modified versions of it (e.g. Wang et al., 1998), the Zhang et al.
77 parameterization (Zhang et al., 2003), the Deposition of O₃ for Stomatal Exchange model (Emberson et al., 2000; Simpson et
78 al., 2012), and the Clean Air Status and Trends Network (CASTNET) deposition estimates (Meyers et al., 1998). The
79 calculation of R_a (mostly based on Monin-Obukhov similarity theory) and R_b across these parameterizations often follow a
80 standard formulation from micrometeorology (Foken, 2006; Wesely and Hicks, 1977, 2000; Wu et al., 2011) and thus does
81 not vary significantly. The main difference between the ozone dry deposition parameterizations lies on the surface resistance
82 R_c . This resistance includes stomatal resistance (R_s), which can be computed by a Jarvis-type multiplicative algorithm (Jarvis,
83 1976) where R_s is the product of its minimum value and a series of response functions to individual environmental conditions.
84 Such conditions typically include air temperature (T), photosynthetically available radiation (PAR), vapour pressure deficit
85 (VPD) and soil moisture (θ), with varying complexity and functional forms.

86

87 Such formalism is empirical in nature and does not adequately represent the underlying ecophysiological processes affect R_s ,
88 (e.g. temperature acclimation). An advance of these efforts includes harmonizing R_s with that computed by land surface models
89 (Ran et al., 2017a; Val Martin et al., 2014), which calculate R_s by coupled photosynthesis-stomatal conductance (A_n-g_s) models
90 (Ball et al., 1987; Collatz et al., 1992, 1991). Such coupling should theoretically give a more realistic account of
91 ecophysiological controls on R_s . Indeed, it has been shown that the above approach may better simulate v_d than the
92 multiplicative algorithms that only considers the effects T and PAR (Val Martin et al., 2014; Wu et al., 2011). The non-stomatal
93 part of R_c often consists of cuticular (R_{cut}), ground (R_g) and other miscellaneous types of resistances (e.g., lower canopy
94 resistance (R_{lc} in Wesely (1989)). Due to very limited measurements and mechanistic understanding towards non-stomatal
95 deposition, non-stomatal resistances are often constants (e.g., R_g) or simply scaled with leaf area index (LAI) (e.g., R_{cut})
96 (Simpson et al., 2012; Wang et al., 1998; Wesely, 1989), while some of the parameterizations (Zhang et al., 2003; Zhou et al.,
97 2017) incorporate the observation of enhanced cuticular O₃ uptake under leaf surface wetness (Altimir et al., 2006; Potier et

98 al., 2015, 2017; Sun et al., 2016). Furthermore, terrestrial atmosphere-biosphere exchange is also directly affected by CO₂, as
99 CO₂ can drive increases in LAI (Zhu et al., 2016) while inhibiting g_s (Ainsworth and Rogers, 2007). These can have important
100 implications on v_d , as shown by Sanderson et al. (2007), where doubling current CO₂ level reduces g_s by 0.5 – 2.0 mm s⁻¹, and
101 by Wu et al. (2012) where v_d increases substantially due to CO₂ fertilization at 2100. Observations from the Free Air CO₂
102 Enrichment (FACE) experiments also confirm CO₂ fertilization and inhibition of g_s effects, but the impacts are variable and
103 species specific such that extrapolation of these effects to global forest cover is cautioned (Norby and Zak, 2011).

104

105 Various efforts have been made to evaluate and assess the uncertainty in modelling ozone dry deposition using field
106 measurements. Hardacre et al. (2015) evaluate the performance of simulated monthly mean v_d and F_{O_3} by 15 chemical transport
107 models (CTM) from the Task Force on Hemispheric Transport of Air Pollutant (TF HTAP) against seven long-term site
108 measurements, 15 short-term site measurements, and modelled v_d from 96 CASTNET sites. This work suggests that the
109 difference in land cover classification is the main source of discrepancy between models. In this case, most of the models in
110 TF HTAP use the same class of dry deposition parameterization (Wang et al., 1998; Wesely, 1989), so a global evaluation of
111 *different* deposition parameterizations was not possible. Also, the focus in this intercomparison study was on seasonal, but not
112 other (e.g. diurnal, daily, interannual) timescales. Using an extended set of measurements, Silva and Heald (2018) evaluate the
113 v_d output from the Wang et al. (1998) parameterization used by the GEOS-Chem chemical transport model. They show that
114 diurnal and seasonal cycles are generally well-captured, while the daily variability is not well-simulated. They find that
115 differences in land type and LAI, rather than meteorology, are the main reason behind model-observation discrepancy at the
116 seasonal scale, and eliminating this model bias results in up to 15% change in surface O₃. This study is also limited to a single
117 parameterization. Using parameterizations that are explicitly sensitive to other environmental variables (e.g. Simpson et al.,
118 2012; Zhang et al., 2003) could conceivably lead to different conclusions.

119

120 Other efforts have been made to compare the performance of different parameterizations. Centoni (2017) find that two different
121 dry deposition parameterizations, Wesely (1989) versus Zhang et al. (2003), implemented in the same chemistry-aerosol model
122 (United Kingdom Chemistry Aerosol model, UKMA), result in up to a 20% difference in simulated surface O₃ concentration.
123 This study demonstrates that uncertainty in v_d can have large potential effect on surface O₃ simulation. Wu et al. (2018)
124 compare v_d simulated by five North-American dry deposition parametrizations to a long-term observational record at a single
125 mixed forest in southern Canada, and find a large spread between the simulated v_d , with no single parameterization uniformly
126 outperforming others. They further acknowledge that as each parameterization is developed with its own set of limited
127 observations, it is natural that their performance can vary considerably under different environments, and advocate for an
128 “ensemble” approach to dry deposition modelling. This highlights the importance of parameterization choice as a key source
129 of uncertainty in modelling ozone dry deposition. Meanwhile, in another evaluation at a single site, Clifton et al. (2017) show
130 that the GEOS-Chem parameterization largely underestimates the interannual variability (IAV) of v_d in Harvard Forest based
131 on the measurement from 1990 to 2000, although they do not show how the IAV of v_d may contribute to the IAV of O₃.

132

133 These developments have made a substantial contribution to our understanding of the importance of O₃ dry deposition in
134 atmospheric chemistry models. Still, pertinent questions remain about the impact of dry deposition model on simulations of
135 the global distribution of ozone and its long-term variability. Here, we build on previous works by posing and answering the
136 following questions:

- 137 1) How does the global distribution of mean v_d vary with different dry deposition parameterizations, and what drives the
138 discrepancies among them? How much might the choice of deposition parameterization affect spatial distribution of
139 surface ozone concentration simulated by a chemical transport model?
- 140 2) How are the IAV and long-term trends of v_d different across deposition parameterizations, and what drives the
141 discrepancies among them? Do they potentially contribute different predictions of the long-term temporal variability
142 in surface ozone?

143 The answers to such question could have important consequences on our ability to predict long-term changes in atmospheric
144 O₃ concentrations as a function of changing climate and land cover characteristics. In general, there is a high computational
145 cost to thorough and large-scale evaluations of different dry deposition parameterizations embedded in CTMs. In this study,
146 we explore these questions using a strategy that combines an offline dry deposition modelling framework incorporating long-
147 term assimilated meteorological and land surface remote sensing data, in combination with a set of CTM sensitivity
148 simulations.

149 **2 Method**

150 **2.1 Dry deposition parameterization**

151 Here we consider several “big-leaf” models commonly used by global chemical transport models. More complex multilayer
152 models require the vertical profiles of leaf area density for different biomes which are generally not available for regional and
153 global models. From the wide range of literature on dry deposition studies, we observe that R_s is commonly modelled through
154 one of the following approaches:

- 155 1) Multiplicative algorithm that considers the effects of LAI, temperature and radiation (Wang et al., 1998).
- 156 2) Multiplicative algorithm that considers the effects of LAI, temperature, radiation and water stress (e.g. Meyers et al.,
157 1998; Pleim and Ran, 2011; Simpson et al., 2012; Zhang et al., 2003).
- 158 3) Coupled A_n - g_s model, which exploit the strong empirical relationship between photosynthesis (A_n) and stomatal
159 conductance (g_s) (e.g. Ball et al., 1987; Lin et al., 2015) and to simulate A_n and $g_s = 1/R_s$ simultaneously (e.g. Ran et
160 al., 2017b; Val Martin et al., 2014).

161 Similarly, their functional dependence of non-stomatal surface resistances can be classified into two classes:

- 162 1) Mainly scaling with LAI, with in-canopy aerodynamics parameterized as function of friction velocity (u^*) or radiation
163 (Meyers et al., 1998; Simpson et al., 2012; Wang et al., 1998)

164 2) Additional dependence of cuticular resistance on relative humidity (Pleim and Ran, 2011; Zhang et al., 2003)

165

166 With these considerations, we identify four common parameterizations that are representative of the types of approaches
167 described above:

168 1) The version of Wesely (1989) with the modification from Wang et al. (1998) (hereafter referred to as W98), which is
169 used extensively in global CTMs (Hardacre et al., 2015) and comprehensively discussed by Silva and Heald (2018).
170 This represents Type 1 in both stomatal and non-stomatal parametrizations.

171 2) The Zhang et al. (2003) parameterization (hereafter referred to as Z03), which is used in many North American air
172 quality modelling studies (e.g. Huang et al., 2016; Kharol et al., 2018) and Canadian Air and Precipitation Monitoring
173 Network (CAPMoN) (e.g. Zhang et al., 2009). This represents Type 2 in both stomatal and non-stomatal
174 parameterizations

175 3) W89 with R_s calculated from a widely-used coupled A_n-g_s model, the Ball-Berry model (hereafter referred to as
176 W98_BB) (Ball et al., 1987; Collatz et al., 1992, 1991), which is similar to that proposed by Val Martin et al. (2014),
177 and therefore the current parameterization in Community Earth System Model (CESM). This represents Type 3 in
178 stomatal and Type 1 in non-stomatal parametrization.

179 4) Z03 with the Ball-Berry model (Z03_BB), which is comparable to the configuration in Centoni (2017) implemented
180 in United Kingdom Chemistry and Aerosol (UKCA) model. This represents Type 3 in stomatal and Type 2 in non-
181 stomatal parametrization.

182

183 Another important consideration in choosing Z03 and W98 is that they both have parameters for all major land types over the
184 globe, making them widely applicable in global modelling. We extract the source code (Wang et al., 1998) and parameters
185 (Baldocchi et al., 1987; Jacob et al., 1992; Jacob and Wofsy, 1990; Wesely, 1989) of W98 from GEOS-Chem CTM
186 (http://wiki.seas.harvard.edu/geos-chem/index.php/Dry_deposition). The source code of Z03 are obtained through personal
187 communication with Zhiyong Wu and Leiming Zhang, which follows the series of papers that described the development and
188 formalism of the parameterization (Brook et al., 1999; Zhang et al., 2001, 2002, 2003). The Ball-Berry A_n-g_s model (Ball et
189 al., 1987; Collatz et al., 1992, 1991; Farquhar et al., 1980) and its solver are largely based on the algorithm of CLM
190 (Community Land Model) version 4.5 (Oleson et al., 2013), which is numerically stable (Sun et al., 2012). We use identical
191 formulae of R_a and R_b (Paulson, 1970; Wesely and Hicks, 1977) for each individual parameterizations, allowing us to focus
192 our analysis on differences in parameterizations of R_c alone. Table S1 gives a brief description on the formalism of each of the
193 dry deposition parameterizations.

194 **2.2 Dry deposition model configuration, inputs, and simulation**

195 The above parameterizations are re-implemented in R language (R core team, 2017) in the modeling framework of the
196 Terrestrial Ecosystem Model in R (<http://www.cuhk.edu.hk/sci/essc/tgabi/tools.html>), and driven by gridded surface

197 meteorology and land surface data sets. The meteorological forcing chosen for this study is the Modern-Era Retrospective
198 Analysis for Research and Application-2 (MERRA-2) (Gelaro et al., 2017), an assimilated meteorological product at hourly
199 time resolution spanning from 1980 to present day. MERRA-2 contains all the required surface meteorological fields except
200 VPD and RH , which can be readily computed from T , specific humidity (q) and surface air pressure (P). We use the CLM land
201 surface dataset (Lawrence and Chase, 2007), which contains information for land cover, per-grid cell coverage of each plant
202 functional type (PFT) and PFT-specific LAI, which are required to drive the dry deposition parameterizations, and soil
203 property, which is required to drive the A_n-g_s model in addition to PFT and PFT-specific LAI. CLM land types are mapped to
204 the land type of W98 following Geddes et al. (2016). The mapping between CLM and Z03 land types are given in Table S2.
205 Other relevant vegetation and soil parameters are also imported from CLM 4.5 (Oleson et al., 2013), while land cover specific
206 roughness length (z_0) values follow Geddes et al. (2016). Leaf is set to be wet when either latent heat flux $< 0 \text{ W m}^{-2}$ or
207 precipitation $> 0.2 \text{ mm hr}^{-1}$. Fractional coverage of snow for Z03 is parameterized as a land-type specific function of snow
208 depth following the original manuscript of Z03, while W98 flags grid cells with albedo > 0.4 or permanently glaciated as
209 snow-covered.

210

211

212 As the IAV of LAI could be an important factor in simulating v_d , the widely-used third generation Global Inventory Modelling
213 and Mapping Studies Leaf Area Index product (GIMMS LAI3g, abbreviated as LAI3g in this paper) (Zhu et al., 2013), which
214 is a global time series of LAI with 15-day temporal frequency and 1/12 degree spatial resolution spanning from late 1981 to
215 2011, is incorporated in this study. We derive the interannual scaling factors that can be applied to scale the baseline CLM-
216 derived LAI (Lawrence and Chase, 2007) for each month over 1982 to 2011. All the input data are aggregated into horizontal
217 resolution of $2^\circ \times 2.5^\circ$ to align with the CTM sensitivity simulation described in the next sub-section. To represent sub-grid
218 land cover heterogeneity, grid cell-level v_d is calculated as the sum of v_d over all sub-grid land types weighted by their
219 percentage coverage in the grid cell (a.k.a tiling or mosaic approach, e.g. Li et al., 2013). This reduces the information loss
220 when land surface data is aggregated to coarser spatial resolution, and allows us to retain PFT-specific results for each grid
221 box in the offline dry deposition simulations.

222

223 We run three sets of 30-years (1982-2011) simulations with the deposition parameterizations to investigate how v_d simulated
224 by different parameterizations responds to different environmental factors over multiple decades. The settings of the
225 simulations are summarized in Table 1. The first set, [Clim], focuses on meteorological variability alone, driven by MERRA-
226 2 meteorology and a multiyear (constant) mean annual cycle of LAI derived from LAI3g. The second set, [Clim+LAI],
227 combines the effects of meteorology and IAV in LAI, driven by the same MERRA-2 meteorology plus the LAI time series
228 from LAI3g. As the increase in atmospheric CO_2 level over multidecadal timescales may lead to significant reduction in g_s as
229 plants tend to conserve water (e.g. Franks et al., 2013; Rigden and Salvucci, 2017), we introduce the third set of simulation,
230 [Clim+LAI+ CO_2], which is driven by varying meteorology and LAI, plus the annual mean atmospheric CO_2 level measured

231 in Mauna Loa (Keeling et al., 2001) (for the first two sets of simulations, atmospheric CO₂ concentration held constant at 390
232 ppm). Since W98 and Z03 do not respond to changes in CO₂ level, only W98_BB and Z03_BB are run with [Clim+LAI+CO₂]
233 to evaluate this impact. We focus on the daytime (solar elevation angle > 20°) v_d , as both v_d and surface O₃ concentration
234 typically peak around this time. We calculate monthly means, filtering out the grid cells with monthly total daytime < 100
235 hours.

236

237 In summary, we present for the first time a unique set of global dry deposition velocity predictions over the last 30 years driven
238 by identical meteorology and land cover, so that discrepancies (in space and time) among the predicted v_d are a result
239 specifically of dry deposition parameterization choice, or assumptions about how land cover is treated in each.

240 **2.3 Chemical transport model sensitivity experiments**

241 We quantify the sensitivity of surface O₃ to variations in v_d using a global 3D CTM, GEOS-Chem version 11.01 (www.geos-
242 chem.org), which includes comprehensive HO_x-NO_x-VOC-O₃-BrO_x chemical mechanisms (Mao et al., 2013) and is widely
243 used to study tropospheric ozone (e.g. Hu et al., 2017; Travis et al., 2016; Zhang et al., 2010). The model is driven by the
244 assimilated meteorological data from the GEOS-FP (Forward Processing) Atmospheric Data Assimilation System (GEOS-5
245 ADAS) (Rienecker et al., 2008), which is jointly developed by National Centers for Environmental Prediction (NCEP) of
246 National Oceanic and Atmospheric Administration (NOAA) and the Global Modelling and Assimilation Office (GMAO). The
247 model is run with a horizontal resolution of 2°×2.5°, and 47 vertical layers. The dry deposition module, which has been
248 discussed above (W98), is driven by the monthly mean LAI retrieved from Moderate Resolution Imaging Spectroradiometer
249 (MODIS) (Myneni et al., 2002) and the 2001 version of Olson land cover map (Olson et al., 2001). Both of the maps are
250 remapped from their native resolutions to 0.25°×0.25°.

251

252 We propose to estimate the sensitivity of surface O₃ concentrations to uncertainty/changes in v_d by the following equation:

253

$$\Delta O_3 = \beta \frac{\Delta v_d}{v_d}$$

254 where ΔO_3 is the response of monthly mean daytime surface O₃ to fractional change in v_d ($\Delta v_d/v_d$), and β accounts for the
255 sensitivity of surface O₃ concentration in a grid box to the perturbation in v_d within that grid box. To estimate β , we run two
256 simulations for the year 2013, one with default setting and another where we perturb v_d by +30%. Thus, this approach could
257 represent a conservative estimate of O₃ sensitivity to v_d if the impacts on other species result in additional effects on O₃. We
258 use this sensitivity to identify areas where local uncertainty and variability in v_d is expected to affect local surface O₃
259 concentration, and we use the assumption of linearity to estimate those impacts to a first order (e.g. Wong et al. 2018). In the
260 Supplemental Methods, we justify this first order assumption mathematically, as well as demonstrate the impact of using a
261 second order approximation, and estimate the uncertainty using an assumption of linearity to be within 30%. However, we
262 note this first-order assumption may not be able to capture the effects of chemical transport, changes in background ozone and

263 non-linearity in chemistry, which can contribute to response of O₃ concentration to v_d . Our experiment could help identify
264 regions where more rigorous modelling efforts could be targeted in future work. We limit our analysis to grid cells where the
265 monthly average v_d is greater than 0.25 cm s⁻¹ in the unperturbed GEOS-Chem simulation, since changes in surface O₃
266 elsewhere are expected to be attributed more to change in background O₃ rather than the local perturbation of v_d (Wong et al.,
267 2018).

268 3. Evaluation of Dry Deposition Parameterizations

269 We first compare our offline simulations of seasonal mean daytime average v_d that result from the four parameterizations in
270 the [Clim] and [Clim+LAI] scenarios with an observational database largely based on the evaluation presented in Silva and
271 Heald (2018). We do not include the evaluation of v_d from [Clim+LAI+CO₂] scenario as we find that the impact of CO₂
272 concentration on v_d is negligible over the period of concern, as we will show in subsequent sections. We use two unbiased and
273 symmetrical statistical metrics, normalized mean bias factor (*NMBF*) and normalized mean absolute error factor (*NMAEF*), to
274 evaluate our parameterizations. Positive *NMBF* indicates that the parameterization overestimates the observations by a factor
275 of $1 + NMBF$ and the absolute gross error is *NMAEF* times the mean observation, while negative *NMBF* implies that the
276 parameterization underestimates the observations by a factor of $1 - NMBF$ and the absolute gross error is *NMAEF* times the
277 mean model prediction (Yu et al., 2006). We use the simulated subgrid land type-specific predictions of v_d that correctly match
278 the land type and the averaging window indicated by the observations. We exclude instances where the observed land type
279 does not have a match within the model grid box. While this removes 1/3 of the original data sets used in Silva and Heald
280 (2018), this means that mismatched land-cover types can be ignored as a factor in model bias.

281

282 Figure 1 shows the fractional coverage within each grid cell and the geographic locations of O₃ flux observation sites for each
283 major land type. Nearly all the observations are clustered in Europe and North America, except three sites in the tropical
284 rainforest and one site in tropical deciduous forest in Thailand. For most major land types, there are significant mismatches
285 between the locations of flux measurements and the dominant land cover fraction, which may hinder the spatial
286 representativeness of our evaluation. The resulting *NMBF* and *NMAEF* for five major land type categories are shown in Table
287 2, and the list of sites and their descriptions are given in Table S3. In general, the numerical ranges of both *NMBF* and *NMAEF*
288 are similar to that of Silva and Heald (2018), and no single parameterization of the four parameterizations outperforms the
289 others across all five major land types.

290

291 The performance metrics of each parameterization at each land type are summarized in table 2. Comparing the two
292 multiplicative parameterizations (W98 and Z03), we find that W98 performs satisfactorily over deciduous forests and
293 tropical rainforests, while strongly underestimating daytime v_d over coniferous forests. In contrast, Z03 performs better in
294 coniferous forests but worse in tropical rainforests and deciduous forests. The severe underestimation of daytime v_d by Z03

295 over tropical rainforests has previously been attributed to persistent canopy wetness, and hence stomatal blocking imposed
296 by the parameterization (Centoni, 2017). We also note that even for the same location, v_d can vary significantly between
297 seasons (Rummel et al., 2007) and management practices (Fowler et al., 2011), which models may fail to capture due to
298 limited representations of land cover. Given the small sample size ($N = 5$), diverse environments, and large anthropogenic
299 intervention in the tropics, the disparity in performance metrics may not fully reflect the relative model performance.
300 Baseline cuticular resistances in Z03 under dry and wet canopy are 1.5 and 2 times that of coniferous forests, respectively
301 (Zhang et al., 2003), such that the enhancement of cuticular uptake by wetness may not compensate the reduced g_s over
302 tropical rainforests, and, to a lesser extent, deciduous forests.

303

304 Over grasslands, W98 has higher positive biases, while Z03 has higher absolute errors. This is because for datasets at high
305 latitudes, the dominant grass PFT is arctic grass, which is mapped to “tundra” land type (Geddes et al., 2016). While tundra
306 is parameterized similarly to grasslands in W98, this is not the case in Z03. Combined with the general high biases at other
307 sites for these parameterizations, the large low biases for “tundra” sites in Z03 lower the overall high biases but leads to
308 higher absolute errors.

309

310 Over croplands, the positive biases and absolute errors are relatively large for both W98 and Z03 (with Z03 performing worse
311 in general than W98). The functional and physiological diversity with the “crop” land type also contributes to the general
312 difficulty in simulating v_d over cropland. Even though Z03 has individual parameterizations for 4 specific crop types (rice,
313 sugar, maize and cotton), this advantage is difficult to fully leverage as most global land cover data sets do not resolve croplands
314 into such detail. Having land cover maps that distinguish between more crop types could potentially improve the performance
315 of Z03. The evaluation for herbaceous land types also suggests that as CLM PFT do not have exact correspondence with W98
316 and Z03 land types, our results over herbaceous land types are subject to the uncertainty in land type mapping (e.g. tundra vs
317 grassland, specific vs generic crops, C3 vs C4 grass).

318

319 Substituting the native g_s in W98 and Z03 by that simulated by Ball-Berry model (the W98_BB and Z03_BB runs) generally,
320 though not universally, leads to improvement in model performance against the observations. W98_BB has considerably
321 smaller biases and absolute errors than W98 over grassland. While having little effect on the absolute error, W98_BB improves
322 the biases over coniferous forest and cropland compared to W98, but worsens the biases over rainforests and deciduous forests.
323 In contrast, Z03_BB is able to improve the model-observation agreement over all 5 land types when compared to Z03. This
324 finding echoes that from Wu et al. (2011), who explicitly show the advantage of replacing the g_s of Wesely (1989) with the
325 Ball-Berry model in simulating v_d over a forest site, and in addition shows the potential of Ball-Berry model in improving
326 spatial distribution of mean v_d . The different responses to substituting native g_s with that from Ball-Berry model highlight the
327 significant differences in parameterizing non-stomatal uptake between W98 and Z03, which further suggests that the
328 uncertainty in non-stomatal deposition should not be overlooked.

329

330 The minimal impact that results from using LAI that matches the time of observation is not unexpected, since the
331 meteorological and land cover information from a $2^\circ \times 2.5^\circ$ grid cell may not be representative of the typical footprint of a site
332 measurement (on the order of 10^{-3} to 10^1 km², e.g. Chen et al., 2009, 2012). The mismatch between model resolution and the
333 footprint of site-level measurements has also been highlighted in previous evaluation efforts in global-scale CTMs (Hardacre
334 et al., 2015; Silva and Heald, 2018). Furthermore, the sample sizes for all land types are small ($N \leq 16$) and the evaluation
335 may be further compromised by inherent sampling biases.

336

337 In addition to the evaluation against field observation, we find good correlation ($R^2 = 0.94$) between the annual mean v_d from
338 GEOS-Chem at 2013 and the 30-year mean v_d of W98 run with static LAI, providing further evidence that our
339 implementation of W98 is reliable. Overall, our evaluation shows that the quality of our offline simulation of dry deposition
340 across the four parameterizations in this work is largely consistent with previous global modelling evaluation efforts.

341 **4. Impact of Dry Deposition Parameterization Choice on Long-Term Averages**

342 Here we summarize the impact that the different dry deposition parameterizations may have on simulations of the spatial
343 distribution of v_d and on the inferred surface O₃ concentrations. We begin by comparing the simulated long-term mean v_d
344 across parameterizations, then use a chemical transport model sensitivity experiment to estimate the O₃ impacts.

345

346 Figure 2 shows the 30-year July daytime average v_d simulated by W98 over vegetated surfaces (defined as the grid cells with
347 $>50\%$ plant cover), and Figure 3 shows the difference between the W98 and the W98_BB, Z03, Z03_BB predictions
348 respectively. We first focus on results from July because of the coincidence of high surface O₃ level, biospheric activity and
349 v_d in the Northern Hemisphere (NH), and will subsequently discuss the result for December, when such condition holds for
350 the Southern Hemisphere (SH). W98 simulates the highest July mean daytime v_d in Amazonia (1.2 to 1.4 cm s⁻¹), followed by
351 other major tropical rainforests, and temperate forests in northeastern US. July mean daytime v_d in other temperate regions in
352 North America and Eurasia typically range from 0.5 to 0.8 cm s⁻¹, while in South American and African savannah, and most
353 parts of China, daytime v_d is around 0.4 to 0.6 cm s⁻¹. In India, Australia, western US, and polar tundra Mediterranean region,
354 July mean daytime v_d is low (0.2 - 0.5 cm s⁻¹).

355

356 The other three parameterizations (W98_BB, Z03, Z03_BB) simulate substantially different spatial distributions of daytime
357 v_d . In North America, we find W98_BB, Z03 and Z03_BB produce lower v_d (by -0.1 to -0.4 cm s⁻¹) compared to W98 in
358 deciduous forest-dominated northeastern US and slightly higher v_d in boreal forest-dominated regions of Canada. Z03 and
359 Z03_BB produce noticeably lower v_d (by up to -0.2 cm s⁻¹) in arctic tundra and grasslands in western US. In southeastern US,
360 W98_BB and Z03_BB simulate a slightly higher v_d (by up to $+0.1$ cm s⁻¹), while Z03 suggests a slightly lower v_d (by up to -

361 0.1 cm s⁻¹). W98_BB simulates a lower (-0.1 to -0.4 cm s⁻¹) v_d in tropical rainforests, with larger reductions concentrated in
362 southern Amazonia, where July is within the dry season, while the northern Amazonia is not (Malhi et al., 2008). Z03 and
363 Z03_BB simulate much smaller (-0.4 to -0.6 cm s⁻¹) v_d in all tropical rainforests.

364

365 Over the midlatitudes in Eurasia, Australia and South America except Amazonia, W98_BB, Z03 and Z03_BB generally
366 simulate a lower daytime v_d by up to 0.25 cm s⁻¹, possibly due to the dominance of grasslands and deciduous forests, where
367 W98 tends to be more high-biased than other parameterizations when compared to the observations of v_d . In southern African
368 savannah, W98_BB and Z03_BB suggest a much lower daytime v_d (by -0.1 to -0.4 cm s⁻¹) because of explicit consideration of
369 soil moisture limitation to A_n and g_s (demonstrated by the spatial overlap with soil moisture stress factors shown in Fig. S2).
370 Z03_BB simulates a particularly high daytime v_d over the high-latitude coniferous forests (+0.1 to +0.3 cm s⁻¹). W98_BB and
371 Z03_BB produce higher daytime daytime v_d (up to +0.15 cm s⁻¹) in India and South China due to temperature acclimation
372 (Kattge and Knorr, 2007), which allows more stomatal opening under the high temperature that would largely shut down the
373 stomatal deposition in W98 and Z03, as long as the soil does not become too dry to support stomatal opening. This is guaranteed
374 by the rainfall from summer monsoon in both regions. Low v_d is simulated by Z03 and Z03_BB in the grasslands near Tibetan
375 plateau because the grasslands are mainly mapped to tundra land type, which typically has low v_d as discussed in section 3.

376

377 Our results suggest that the global distribution of simulated mean v_d depends substantially on the choice of dry deposition
378 parameterization, driven primarily by the response to hydroclimate-related parameters such as soil moisture, VPD and leaf
379 wetness, in addition to land type-specific parameters, which could impact the spatial distribution of surface ozone predicted
380 by chemical transport models. To estimate the impact on surface ozone of an individual parameterization “ i ” compared to the
381 W98 predictions (which we use as a baseline), we apply the following equation:

382
$$\Delta O_{3,i} \approx \beta \frac{\Delta \overline{v_{d,i}}}{\overline{v_{d,W98}}} \quad (3)$$

383 where $\Delta O_{3,i}$ is the estimated impact on simulated O₃ concentrations in a grid box, $\Delta \overline{v_{d,i}}$ is the difference between
384 parameterization i and W98 simulated mean daytime v_d in that grid box, $\overline{v_{d,W98}}$ is W98 output mean daytime v_d for that grid
385 box, and β is the sensitivity of surface ozone to v_d calculated by the method outlined in Section 2.3

386

387 Figure 4 shows the resulting estimates of ΔO_3 globally. We find ΔO_3 is the largest in tropical rainforests for all the
388 parameterizations (up to 5 to 8 ppbv). Other hotspots of substantial differences are boreal coniferous forests, eastern US,
389 continental Europe, Eurasian steppe and the grassland in southwestern China, where ΔO_3 is either relatively large or the signs
390 disagree among parameterizations. In India, Indochina and South China, ΔO_3 is relatively small but still reaches up to up to -
391 2 ppbv. We find that ΔO_3 is not negligible (1-4 ppbv) in many regions with relatively high population density, which suggests
392 that the choice of dry deposition parameterization can be relevant to the uncertainty in the study of air quality and its implication
393 on public health. We note that we have not estimated ΔO_3 for some regions with low GEOS-Chem-predicted v_d (< 0.25 cm s⁻¹)

394 ¹, as described in section 2.3), but where the disagreement in v_d between parameterizations can be large (e.g., southern African
395 savannah, see Figure 3). Given this limitation, the impacts on O_3 we have summarized may therefore be spatially conservative.
396

397 To explore the impact of different prediction of v_d on surface O_3 in different seasons, we repeat the above analyses for
398 December. Figure 5 shows the 1982-2011 mean December daytime v_d predicted by W98, while Figure 6 shows the difference
399 between W98 and the Z03, W98_BB, Z03_BB respectively. High latitudes in the NH are excluded due to the small number of
400 daytime hours. Z03 and Z03_BB simulate substantially lower in daytime v_d at NH midlatitudes because Z03 and Z03_BB
401 allow partial snow cover but W98 and W98_BB only allow total or no snow cover. At midlatitudes, the snow cover is not high
402 enough to trigger the threshold of converting vegetated to snow covered ground in W98 and W98_BB, resulting in lower
403 surface resistance, and hence higher daytime v_d comparing to Z03 and Z03_BB; in Amazonia, the hotspot of difference in
404 daytime v_d shifts from the south to the north relative to July, which is in the dry season (Malhi et al., 2008). These results for
405 December, together with our findings from July, suggest that the discrepancy in simulated daytime v_d between W98 and other
406 parameterizations is due to the explicit response to hydroclimate in the former compared to the latter. Given that field
407 observations indicate a large reduction of v_d in dry season in Amazonia (Rummel et al., 2007), the lack of dependence of
408 hydroclimate can be a drawback of W98 in simulating v_d in Amazonia.
409

410 Figure 7 shows the resulting estimates of ΔO_3 globally for December using Equation 3. In all major rainforests, ΔO_3 is smaller
411 in December due to generally lower sensitivity compared to July. A surprising hotspot of both daytime Δv_d and ΔO_3 is the
412 rainforest/tropical deciduous forest in Myanmar and its eastern bordering region, which also has distinct wet and dry season.
413 The proximity of December to the dry season, which starts at January (e.g. Matsuda et al., 2005), indicates that the consistent
414 Δv_d between W98 and other parameterizations is driven by hydroclimate as in Amazonia. Comparison with field measurements
415 (Matsuda et al., 2005) suggests that the W98_BB and Z03_BB capture daytime v_d better than W98, while Z03 may
416 overemphasize the effect of such dryness. The above reasoning also explains some of the Δv_d in India and south China across
417 the three parameterizations. These findings identify hydroclimate as a key driver of process uncertainty of v_d over tropics and
418 subtropics, and therefore its impact on the spatial distribution of surface ozone concentrations, independent of land type-based
419 biases, in these regions.
420

421 Overall, these results demonstrate that the discrepancy in the spatial distribution of simulated mean daytime v_d resulting from
422 choice of dry deposition parameterization can have an important impact on the global distribution of surface O_3 predicted by
423 chemical transport models. We find that the response to hydroclimate by individual parametrization not only affects the mean
424 of predicted surface ozone, but also has different impacts in different seasons, which is complementary to the findings of
425 Kavassalis and Murphy (2017) that mainly focus on how shorter-term hydrometeorological variability may modulate surface
426 O_3 through dry deposition.
427

428 5. Impact of Dry Deposition Parameterization Choice on Trends and Interannual Variability

429 Here we explore the impact that different dry deposition parameterizations may have on predictions of IAV and trends in v_d
430 and on the inferred surface O_3 concentrations. We use the Theil-Sen method (Sen, 1968), which is less susceptible to outliers
431 than least-square methods, to estimate trends in July daytime v_d (and any underlying meteorological variables), and use p-value
432 < 0.05 to estimate significance.

433
434 Figure 8 shows the trend in July mean daytime v_d from 1982-2011 predicted by each of the parameterizations and scenarios
435 ([Clim], [Clim + LAI], and [Clim + LAI + CO₂]). Figure 9 shows the potential impact of these trends in v_d on July daytime
436 surface ozone, which we estimate to a first order using the following equation:

$$437 \quad \Delta O_{30y,i} \approx \beta \times m_{v_d,i} \times 30 \quad (4)$$

438 where $\Delta O_{30y,i}$ and $m_{v_d,i}$ are the absolute change in ozone inferred to a first order as a result of the trend of v_d and the normalized
439 Theil-Sen slope (% yr⁻¹) of v_d , for parameterization i over the 30-years (1982-2011).

440
441 In [Clim] simulations (where LAI is held constant), significant decreasing trends in July daytime v_d are simulated by the Z03,
442 W98_BB and Z03_BB Mongolia, where significant increasing trend in T (warming) and decreasing trend in RH (drying)
443 detected in the MERRA-2 surface meteorological field in July daytime. This trend is not present in the W98 parameterization
444 as this formulation does not respond to the long-term drying. We find some decreasing trends in v_d across parts of central
445 Europe and the Mediterranean to varying degrees across the parameterizations. In the SH, we find consistent decreasing trends
446 across all four parameterizations in southern Amazonia and southern African savannah due to warming and drying, which we
447 estimate could produce a concomitant increase in July mean surface ozone of between 1 to 3 ppbv (Figure 9).

448
449 In [Clim+LAI] scenario, all four parameterizations simulate a significant increasing trend of v_d over high latitudes, which is
450 consistent with the observed greening trend over the region (Zhu et al., 2016). We estimate this could produce a concomitant
451 decrease in July mean surface ozone of between 1 to 3 ppbv. The parameterizations generally agree in terms of the spatial
452 distribution of these trends in O_3 . Exceptions include a steeper decreasing trend in most of Siberia predicted by W98, while
453 the trend is more confined in the eastern and western Siberia in the other three parameterizations. Including the effect of CO₂-
454 induced stomatal closure ([Clim+LAI+CO₂] runs) partially offset the increase of v_d in high latitudes, but does not lead to large
455 changes in both the magnitudes and spatial patterns of v_d trend. We find negligible trends in daytime v_d for December in all
456 cases. These results show that across all dry deposition model parameterizations, LAI and climate, more than increasing CO₂,
457 can potentially drive significant long-term changes in v_d and should not be neglected when analyzing the long-term change in
458 air quality over 1982-2011. We note that the importance of the CO₂ effect could grow as period of study further extend to
459 allow larger range of atmospheric CO₂ concentration (Hollaway et al., 2017; Sanderson et al., 2007).

460

461 We go on to explore the impact of parameterization choice in calculations of IAV in v_d . Figure 10 shows the coefficient of
462 variation of linearly detrended July daytime v_d (CV_{v_d}). Figure 11 shows the potential impact this has on IAV in surface ozone,
463 which we estimate to a first order by the following equation:

$$464 \quad \sigma_{O_3,i} \approx \beta \times CV_{v_d,i} \quad (5)$$

465 where $\sigma_{O_3,i}$ is the estimated interannual standard deviation in surface ozone resulting from IAV in v_d given predicted by dry
466 deposition parameterization i . In both cases, we show only the [Clim] and [Clim+LAI] runs, since IAV in CO_2 has negligible
467 impact on interannual variability in v_d .

468

469 Using the W98 parameterization, IAV in predicted v_d and O_3 is considerably smaller in the [Clim] run than that for the [Clim
470 + LAI] run, since both the stomatal and non-stomatal conductance in W98 are assumed to be strong functions of LAI rather
471 than meteorological conditions. This implies that long-term simulations with W98 and constant LAI can potentially
472 underestimate the IAV of v_d and surface ozone. In contrast, IAV in v_d calculated by the Z03 parameterization is nearly the
473 same for the [Clim] and [Clim+LAI] runs. In Z03, g_s is also directly influenced by VPD in addition to temperature and radiation,
474 and non-stomatal conductance in Z03 is much more dependent on meteorology than W98, leading to high sensitivity to climate.
475 Though the Ball-Berry model also responds to meteorological conditions, it considers relatively complex A_n - g_s regulation and
476 includes temperature acclimation, which could dampen its sensitivity to meteorological variability compared to the direct
477 functional dependence on meteorology in the Z03 multiplicative algorithm. Thus, the climate sensitivity of W98_BB and
478 Z03_BB is in between Z03 and W98, as is indicated by more moderate difference between $\sigma_{O_3,i}$ from [Clim] and [Clim+LAI]
479 runs in Figure 11.

480

481 For regional patterns of CV_{v_d} and σ_{O_3} , we focus on the [Clim+LAI] runs (Fig. 10e to 10h and Fig. 11e to 11h) as they allow for
482 a comparison of all 4 parameterizations and contain all the important factors of controlling v_d . In North America, we estimate
483 modest IAV in v_d across all 4 parameterizations ($CV_{v_d} < 15\%$) in most places. We find this results in relatively low σ_{O_3} in
484 northeastern US, and larger σ_{O_3} in central and southeast US (in the range of 0.3 to 2 ppbv). These results are of a similar
485 magnitude to the standard deviation of summer mean background ozone suggested by Fiore et al. (2014) over similar time
486 period, suggesting that IAV of dry deposition can be a potentially important component of the IAV of surface ozone in
487 summer over North America.

488

489 All parameterizations produce larger CV_{v_d} (and therefore larger σ_{O_3}) in southern Amazonia compared to northern and central
490 Amazonia, but we find substantial discrepancies across parameterizations. The estimated impact on IAV in O_3 (σ_{O_3}) in southern
491 Amazonia ranges from less than 1 ppbv predicted by the W98 and W98_BB parameterizations, to exceeding 1.5 - 2.5 ppbv
492 predicted by the Z03 parameterization. IAV is also relatively large in central Africa. We find that the parameterizations which
493 include a Ball-Berry formulation (W98_BB and Z03_BB) estimate higher IAV in this region (with σ_{O_3} varying between 1 to
494 4 ppbv), compared to the W98 and Z03 parameterizations (σ_{O_3} up to 2ppbv). We also note that the Ball-Berry formulations

495 show more spatial heterogeneity compared to W98 and Z03. In our implementation of the Ball-Berry model, impact of soil
496 moisture on g_s is parameterized as a function of root-zone soil matric potential, which makes g_s very sensitive to variation in
497 soil wetness when the its climatology is near the point that triggers limitation on A_n and g_s . Given the large uncertainty in
498 global soil property map (Dai et al., 2019), such sensitivity could be potentially artificial, which should be taken into
499 consideration when implementing Ball-Berry parameterizations in large-scale models despite their relatively good
500 performance in site-level evaluation (Wu et al., 2011).

501

502 Across Europe, the magnitude of IAV predicted by all four parameterizations show relatively good spatial consistency.
503 Simulated CV_{vd} is relatively low in western and northern Europe (<10%), which we estimate translates to less than 1 ppbv of
504 σ_{O_3} . We find larger CV_{vd} (and therefore large σ_{O_3}) over parts of southern Russia and Siberia (σ_{O_3} up to 2.5 ppbv) from all
505 parameterizations except W98. The local geographic distribution of CV_{vd} and σ_{O_3} also significantly differs among the
506 parameterizations. Z03 and Z03_BB simulate larger CV_{vd} in eastern Siberia than W98_BB, while W98_BB and Z03_BB predict
507 larger CV_{vd} over the southern Russian steppe than Z03. Finally, all four parameterizations estimate relatively low CV_{vd} and σ_{O_3}
508 in India, China and Southeast Asia.

509

510 We compare the simulated IAV July CV_{vd} from all four deposition parameterizations with those recorded by publicly available
511 long-term observations. Hourly v_d is calculated using eq. (1) from raw data. We filter out the data points with extreme (> 2 cm
512 s^{-1}) or negative v_d , and without enough turbulence ($u_* < 0.25$ m s^{-1}). As v_d in each daytime hours are not uniformly sampled in
513 the observational datasets, we calculate the mean diurnal cycle, and then calculate the daytime average July of v_d for each year
514 from the mean diurnal cycle, from which CV_{vd} can be calculated.

515 The IAV predicted by all four parameterizations at Harvard Forest is between 3% to 7.9%, which is 2 to 6 times lower than
516 that presented in the observations (18%). We find similar underestimates by all four parameterizations compared to the long-
517 term observation from Hyttiala (Junninen et al., 2009; Keronen et al., 2003; <https://avaa.tdata.fi/web/smart/smear/download>),
518 where observed CV_{vd} (16%) is significantly higher than that predicted by the deposition parameterizations (3.5% - 7.1%). In
519 Blodgett Forest we find that the models underestimate the observed annual CV_{vd} more seriously ($\sim 1\% - 3\%$ compared to 18%
520 in the observations). This suggests that the IAV of v_d may be underestimated across all deposition parameterizations we
521 investigated (and routinely used in simulations of chemical transport). Clifton et al. (2019) attribute this to the IAV in
522 deposition to wet soil and dew-wet leaves, and in-canopy chemistry under stressed condition for forests over northeastern U.S.
523 Some of these processes (e.g. in-canopy chemistry, wetness slowing soil ozone uptake) are not represented by existing
524 parameterizations, contributing to their difficulty in reproducing the observed IAV. The scarcity of long-term ozone flux
525 measurements (Fares et al., 2010, 2017; Munger et al., 1996; Rannik et al., 2012) limits our ability to benchmark the IAV in
526 our model simulations with observational datasets.

527

528 In summary, when both the variability in LAI and climate are considered, the IAV in simulated v_d translates to IAV in surface
529 O_3 of 0.5 – 2ppbv in July for most regions. Such variability is predicted to be particularly strong in southern Amazonian and
530 central African rainforest, where the predicted IAV in July surface O_3 due to dry deposition can be as high as 4 ppbv. This
531 suggests that IAV of v_d can be an important part of the natural variability of surface O_3 . The estimated magnitude of IAV is
532 also dependent of the choice of v_d parameterization, which highlights the importance of v_d parameterization choice on
533 modelling IAV of surface O_3 .

534 **6 Discussion and Conclusion**

535 We present the results of multidecadal global modelling of ozone dry deposition using four different ozone deposition
536 parameterizations that are representative of the major types of approaches of gaseous dry deposition modelling used in global
537 chemical transport models. The parameterizations are driven by the same assimilated meteorology and satellite-derived LAI,
538 which minimizes the uncertainty of model input across parameterization and simplifies interpretation of inter-model
539 differences. The output is evaluated against field observations and shows satisfactory performance. One of our main goals was
540 to investigate the impact of dry deposition parameterization choice on long-term averages, trends, and IAV in v_d over a
541 multidecadal timescale, and estimate the potential concomitant impact on surface ozone concentrations to a first order using a
542 sensitivity simulation approach driven by the GEOS-Chem chemical transport model.

543

544 We find that the performance of the four dry deposition parameterizations against field observations varies considerably over
545 land types, and these results are consistent with other evaluations, reflecting the potential issue that dry deposition
546 parameterizations can often be overfit to a particular set of available observations, requiring caution in their application at
547 global scales. We also find that using more ecophysiological realistic output g_s predicted by the Ball-Berry model can
548 generally improve model performance, but at the cost of high sensitivity to relatively unreliable soil data. However, the number
549 of available datasets of ozone dry deposition observation are still small and concentrated in North America and Europe. We
550 know of only one multi-season direct observational record in Asia (Matsuda et al., 2005) and none in Africa, where air quality
551 can be an important issue. To better constrain regional O_3 dry deposition, effort must be made in making new observations of
552 gaseous dry deposition (Fares et al., 2017) especially in the under-sampled regions. Evaluation and development of ozone dry
553 deposition parameterizations will continue to benefit from publicly available ozone flux measurements and related
554 micrometeorological variables that allow for partitioning measured flux into individual deposition pathways (e.g. Clifton et
555 al., 2017, 2019; Fares et al., 2010; Wu et al., 2011, 2018)..

556

557 We find substantial disagreement in the spatial distribution between the mean daytime v_d predicted by the different
558 parameterizations we tested. We find that these discrepancies are in general a function of both location and season. In NH
559 summer, v_d simulated by the 4 parameterizations are considerably different in many regions over the world. We estimate that

560 this could lead to around 2 to 5 ppbv in uncertainty of surface ozone concentration simulations over a vast majority of land in
561 the NH. In tropical rainforests, where leaf wetness is prevalent and the dry-wet season dynamics can have large impact on v_d
562 (Rummel et al., 2007), we estimate the uncertainty due to dry deposition model choice could even lead to an uncertainty in
563 surface ozone of up to 8 ppbv. We also find noticeable impacts in parameterization choice during SH summer, but we note
564 that due to the unreliability of β at low v_d , we have not assessed its impact on surface ozone in many high-latitude regions of
565 the NH. In general, we find hydroclimate to be an important driver of the uncertainty. This demonstrates that the potential
566 impact of parameterization choice (or, process uncertainty) of v_d is neither spatiotemporally uniform nor negligible in many
567 regions over the world. More multi-seasonal observations are especially needed over seasonally dry ecosystems where the role
568 of hydroclimate in deposition parameterizations need to be evaluated. Recently, standard micrometeorological measurements
569 have been used to derive g_s and stomatal deposition of O_3 over North America and Europe (Ducker et al., 2018), highlighting
570 the potential of using global networks of micrometeorological observation (e.g. FLUXNET (Baldocchi et al., 2001)) to
571 benchmark and calibrate g_s of drydeposition parameterizations, which could at least increase the spatiotemporal
572 representativeness, if not the absolute accuracy, of dry deposition parameterizations, since it would be difficult to constrain
573 non-stomatal sinks with this method. Further research is required to more directly verify whether better constrained g_s leads to
574 improved v_d simulation.

575

576 Over the majority of vegetated regions in the NH, we estimate the IAV of mean daytime v_d is generally on the order of 5 to
577 15% and may contribute between 0.5 to 2 ppbv of IAV in July surface O_3 over the thirty-year period considered here, with
578 each parameterization simulating different geographic distribution of where IAV is highest. The predicted IAV from all four
579 models is smaller than what long-term observations suggest, but its potential contribution to IAV in O_3 is still comparable to
580 the long-term variability of background ozone over similar timescales in U.S. summer (Brown-Steiner et al., 2018; Fiore et al.,
581 2014). This would seem to confirm that v_d may be a substantial contributor to natural IAV of O_3 in summer, at least in U.S. In
582 the southern Hemisphere, the IAV mainly concentrates in the drier part of tropical rainforests. The Ball-Berry
583 parameterizations simulate large and spatially discontinuous CV_{v_d} and σ_{O_3} due to their sensitivity to soil wetness. Globally, we
584 find that IAV of v_d in W98 is mostly driven by LAI, while in other parameterizations climate generally plays a more important
585 role. We therefore emphasize that temporal matching of LAI is important for consistency when W98 is used in long-term
586 simulations. While our results show notable impacts across the globe, in many regions there are no available long-term
587 observation to evaluate the model predictions over interannual timescales. This information is helpful in designing and
588 identifying sources of error in model experiments that involve variability of v_d .

589

590 We are also able to detect statistically significant trends in July daytime v_d over several regions. The magnitudes of trends are
591 up to 1% per year and both climate and LAI contribute to the trend. All four deposition parameterizations identify three main
592 hotspots of decreasing July daytime v_d (southern Amazonia, southern African savannah, Mongolia), which we link mainly to
593 increasing surface air temperature and decreasing relative humidity. Meanwhile, extensive areas at high latitudes experience

594 LAI-driven increasing July daytime v_d , consistent with the greening trend in the region (Zhu et al., 2016). We don't find a
595 strong influence of CO₂-induced stomatal closure in the trend over this time period. Over the 30-years we estimate the trend
596 in July daytime v_d could translate approximately to 1 to 3 ppbv of ozone changes in the areas of impact, indicating the potential
597 effect of long-term changes in v_d on surface ozone. This estimate should be considered conservative, since we are unable to
598 reliably test the sensitivity of ozone to regions with low v_d with our approach.

599

600 While the approach we have presented here allows us to explore the role of dry deposition parameterization choice on
601 simulations of long-term means, trends, and IAV in ozone dry deposition velocity, there remain some limitations and
602 opportunities for development. First, we only used one LAI and assimilated meteorological product. The geographic
603 distribution of trend and IAV of v_d may vary considerably as the LAI and meteorological products used due to their inherent
604 uncertainty (e.g. Jiang et al., 2017). While we expect the qualitative conclusions about how LAI and climate controls the
605 modelled trend and IAV of v_d to be robust to the choice of data set, the magnitude and spatial variability could be affected.
606 Second, the estimated effects on surface O₃ are a first-order inference based on a linear approximation of the impact that v_d
607 has directly on O₃. We have not applied our analysis to regions with low GEOS-Chem v_d , where other components of
608 parameterization (e.g. definition and treatment of snow cover, difference in ground resistance) may have major impact on v_d
609 prediction (Silva and Heald, 2018), nor accounted for the role that v_d variability can have on other chemical species which
610 would have feedbacks on O₃. Moreover, the sensitivity of surface ozone to v_d may be dependent on the choice of chemical
611 transport model (here, the GEOS-Chem model has been used), and possibly the choice of simulation year for the sensitivity
612 simulation. Finally, we have neglected the effect of land use and land cover change on global PFT composition at this stage,
613 which can be another source of variability for v_d , and even long-term LAI retrieval (Fang et al., 2013). Nevertheless, the
614 relatively high *NMAEF* of simulated v_d and the inherent uncertainty in input data (land cover, soil property, assimilated
615 meteorology and LAI) are considered as the major source of uncertainty in our predictions of v_d .

616

617 The impact of dry deposition parameterization choice may also have impacts which we have not explored in this study on
618 other trace gases with deposition velocity controlled by surface resistance, and for which stomatal resistance is an important
619 control of surface resistance (e.g. NO₂). As v_d has already been recognized as a major source of uncertainty in deriving global
620 dry deposition flux of NO₂ and SO₂ (Nowlan et al., 2014), systematic investigation on the variability and uncertainty of v_d for
621 other relevant chemical species does not only contribute to understanding the role of gaseous dry deposition on air quality, but
622 also to biogeochemical cycling. Particularly, gaseous dry deposition has been shown to be a major component in nitrogen
623 deposition (Geddes and Martin, 2017; Zhang et al., 2012), highlighting the potential importance of understanding the role of
624 v_d parameterization in modelling regional and global nitrogen cycles.

625

626 Here we have built on the recent investigations of modelled global mean (Hardacre et al., 2015; Silva and Heald, 2018) and
627 observed long-term variability (Clifton et al., 2017) of O₃ v_d . We are able to demonstrate the substantial impact of v_d

628 parameterization on modelling the global mean and IAV of v_d , and their non-trivial potential impact on simulated seasonal
629 mean and IAV of surface ozone. We demonstrate that the parameterizations with explicit dependence on hydroclimatic
630 variables have higher sensitivity to climate variability than those without. Lin et al. (2019) likewise recently demonstrated the
631 importance of accounting for water availability in O3 dry deposition modeling. Difficulties in evaluating predictions of v_d for
632 many regions of the world (e.g. most of Asia and Africa) persist due to the scarcity of measurements. This makes a strong case
633 for additional measurement and model studies of ozone dry deposition across different timescales, which would be greatly
634 facilitated by an open data sharing infrastructure (e.g. Baldocchi et al., 2001; Junninen et al., 2009).

635 **Code Availability**

636 The source code and output of the dry deposition parameterizations can be obtained by contacting the corresponding author
637 (jgeddes@bu.edu).

638

639 **Competing Interests**

640 The authors declare no competing interests.

641 **Author Contributions**

642 AYHW and JAG developed the ideas behind this study, formulated the methods, and designed the model experiments. AYHW
643 wrote the dry deposition code and ran the chemical transport model simulations. Data analysis was performed by AYHW, with
644 input and feedback from JAG. APKT provided the photosynthesis model code, and co-supervised the dry deposition code
645 development. SJS compiled the dry deposition observations used for evaluation. Manuscript preparation was performed by
646 AYHW, reviewed by JAG, and commented, edited, and approved by all authors.

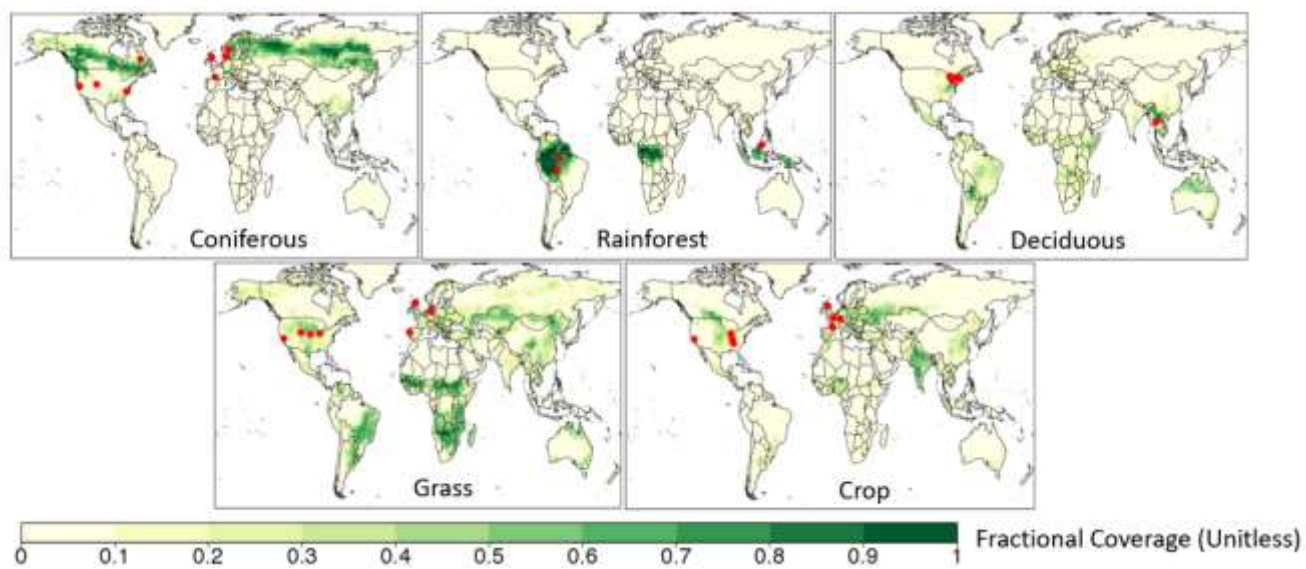
647 **Acknowledgement**

648 This work was funded by an NSF CAREER grant (ATM-1750328) to project PI J.A. Geddes; and the Vice-Chancellor
649 Discretionary Fund (Project ID: 4930744) from The Chinese University of Hong Kong (CUHK) given to the Institute of
650 Environment, Energy and Sustainability. Funding support to SJS was provide by a National Science Foundation grant to C.L.
651 Heald (ATM-1564495). We also thank the Global Modelling and Assimilation Office (GMAO) at NASA Goddard Flight
652 Center for providing the MERRA-2 data, Ranga Myneni for GIMMS LAI3g product, Petri Keronen and Ivan Mammarella for
653 the flux measurements in Hyytiala, Silvano Fares and Allen Goldstein for the flux measurement in Blodgett Forest, and
654 Leiming Zhang and Zhiyong Wu for the source code of Z03.

655

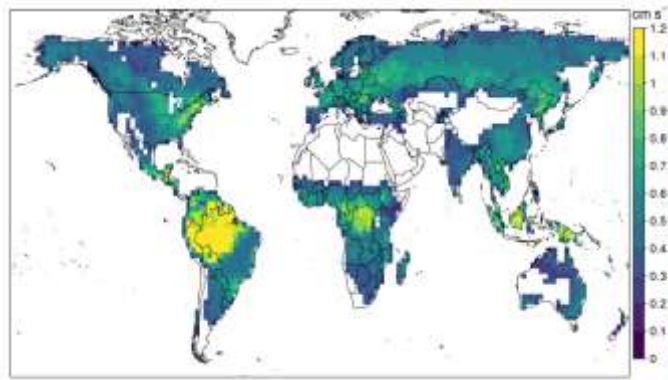
656

657
658
659
660
661
662
663
664
665
666
667
668
669



670
671
672

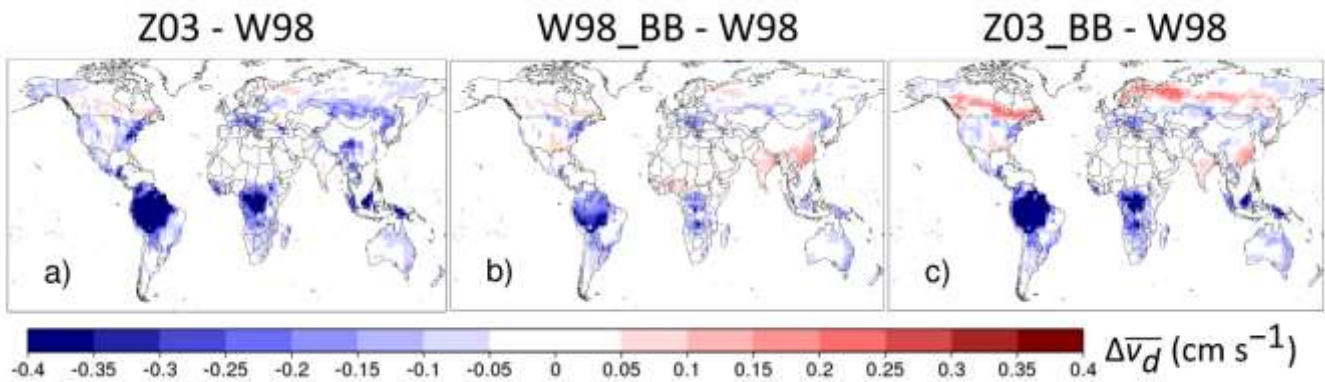
Figure 1: Fractional coverage of each major land type at each grid cell. Blue dots indicate the locations of the observational sites.



673

674 **Figure 2:** 1982-2011 July mean daytime v_d (solar elevation angle $> 20^\circ$) over vegetated land surface simulated by W98.

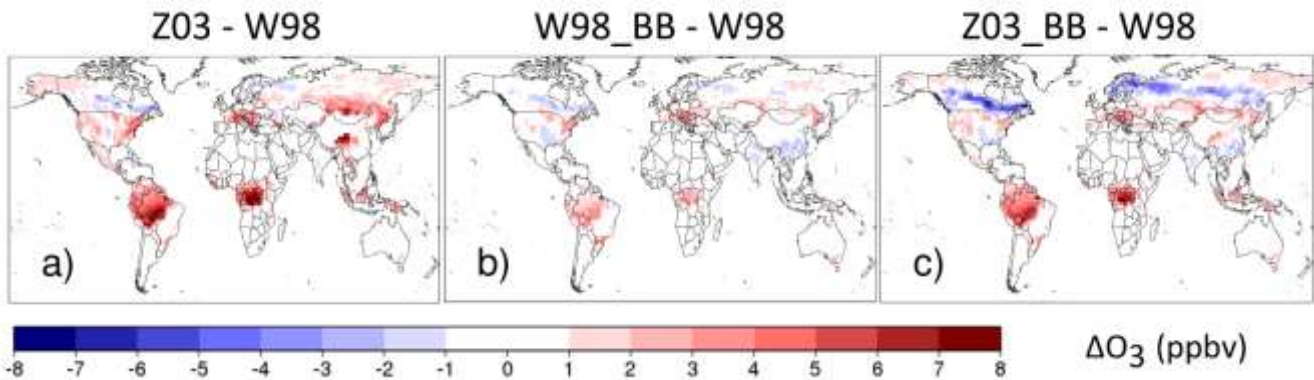
675



676

677 **Figure 3:** Differences of 1982-2011 July mean daytime v_d ($\Delta \bar{v}_d$) between three other parameterizations (Z03, W98_BB and
678 Z03_BB) and W98 over vegetated land surface.

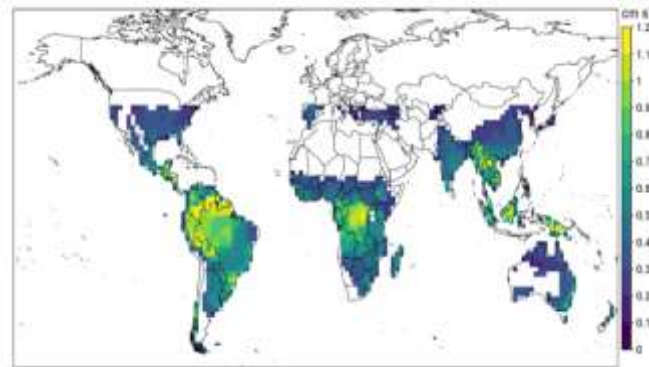
679



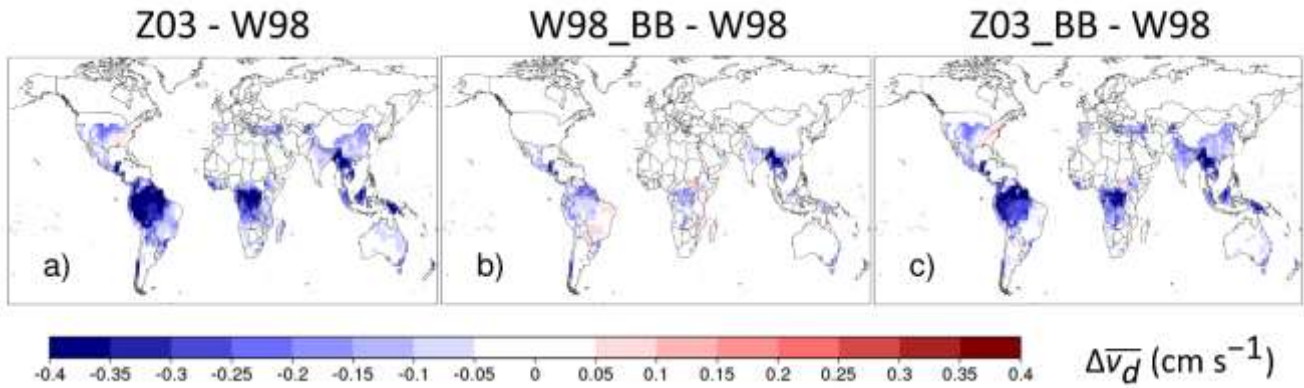
680

681 **Figure 4:** Estimated difference in July mean surface ozone (ΔO_3) due to the discrepancy of simulated July mean daytime v_d
682 among the parameterizations.

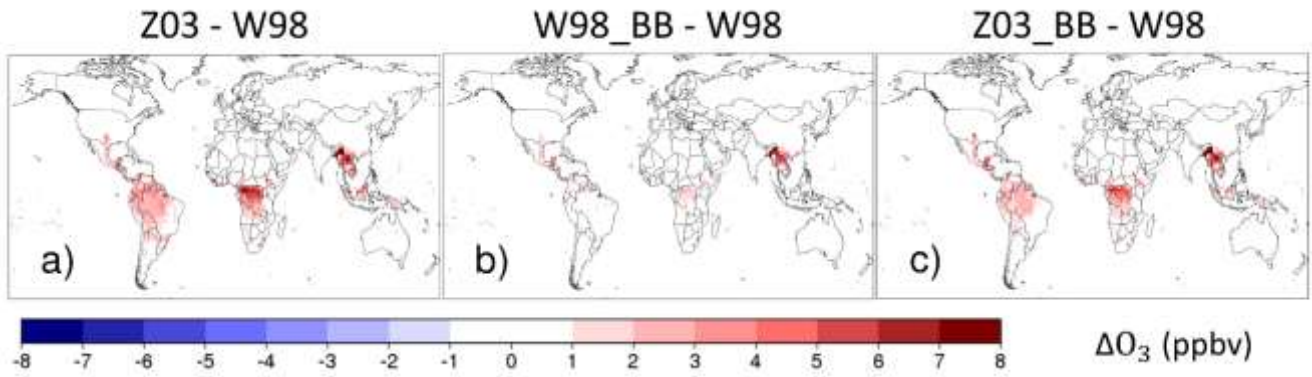
683
684
685
686



687
688 **Figure 5:** 1982-2011 December mean daytime v_d (solar elevation angle $> 20^\circ$) over vegetated land surface simulated by
689 W98. The data over high latitudes over Northern Hemisphere is invalid due to insufficient daytime hours over the month ($<$
690 100 hours month $^{-1}$)
691

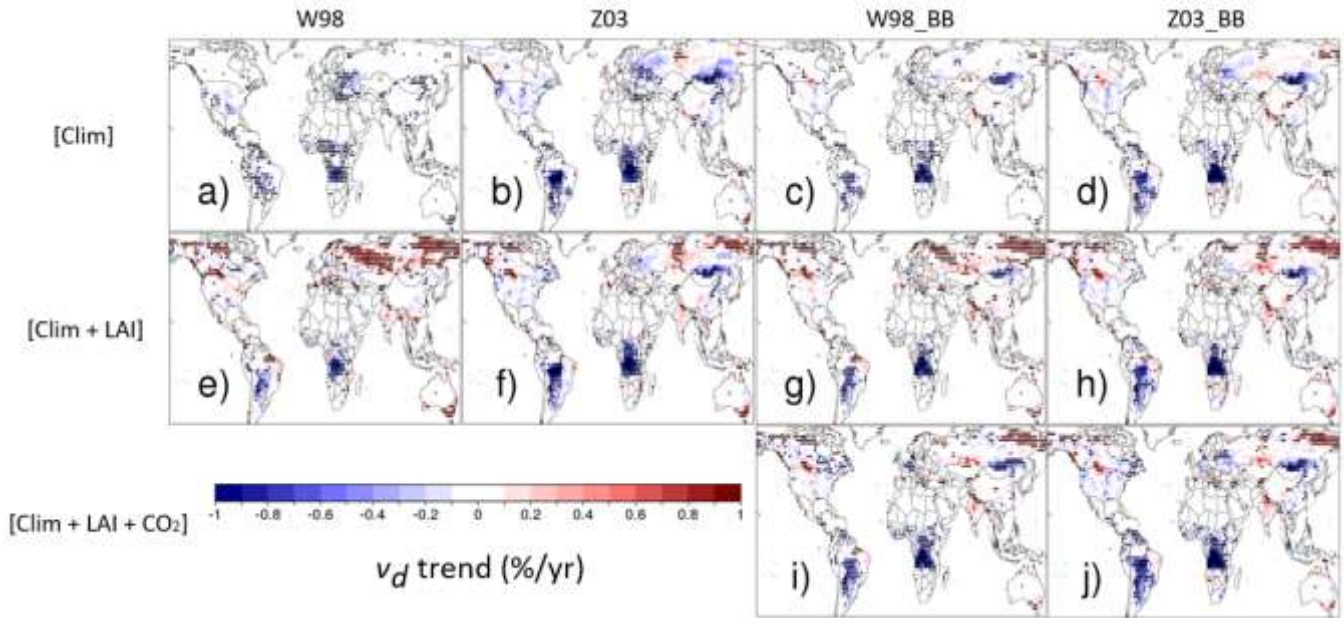


692
693 **Figure 6:** Differences of 1982-2011 December mean daytime v_d ($\Delta\bar{v}_d$) between three other parameterizations (Z03, W98_BB
694 and Z03_BB) and W98 over vegetated land surface.
695
696

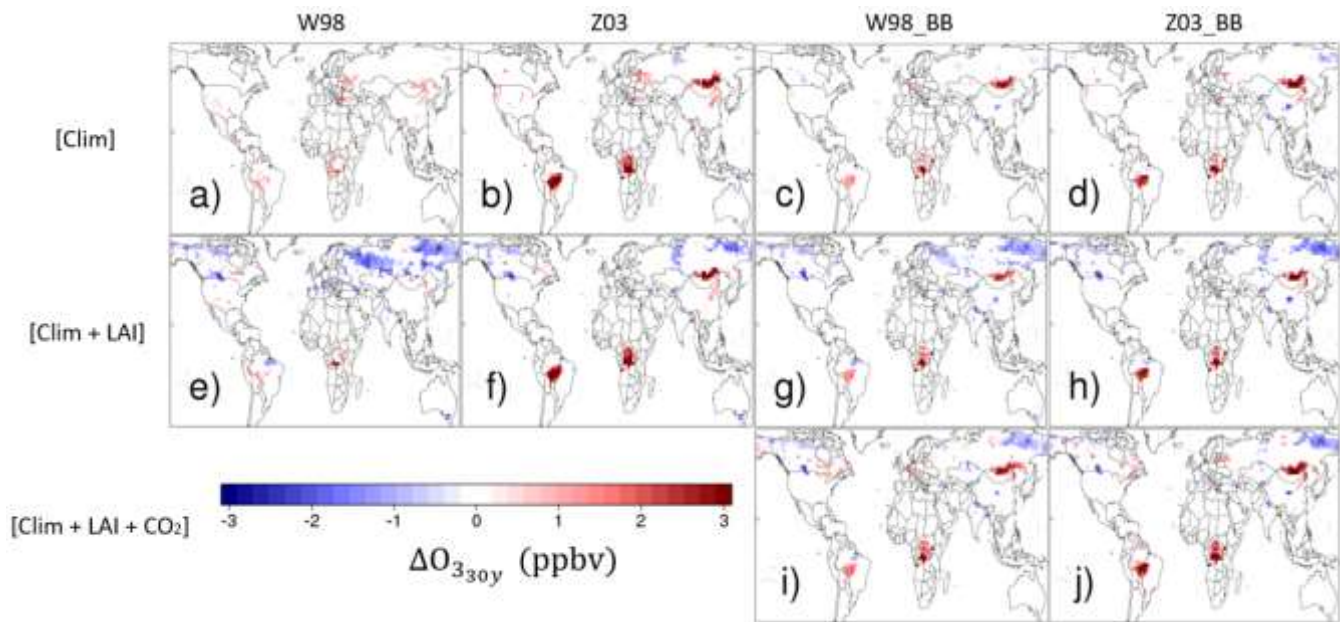


697
 698 **Figure 7:** Estimated difference in December mean surface ozone (ΔO_3) due to the discrepancy of simulated December mean
 699 daytime v_d among the parameterizations.

700
 701



702
 703 **Figure 8:** Trends of July mean daytime v_d during 1982-2011 over vegetated land surface. Black dots indicate statistically
 704 significant trends ($p < 0.05$)



705

706

Figure 9: Estimated impact of trends of July mean daytime v_d on July mean surface ozone during ($\Delta O_{3\ 30y}$) 1982-2011 over

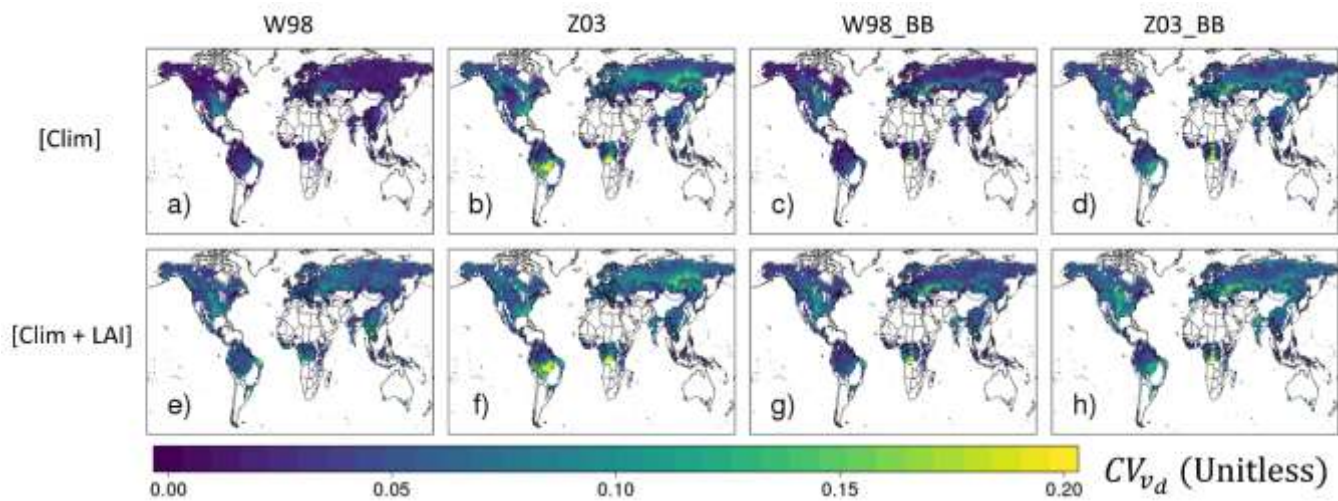
707

vegetated land surface. Only grid points with statistically significant trends ($p < 0.05$) in July mean daytime v_d are

708

considered.

709



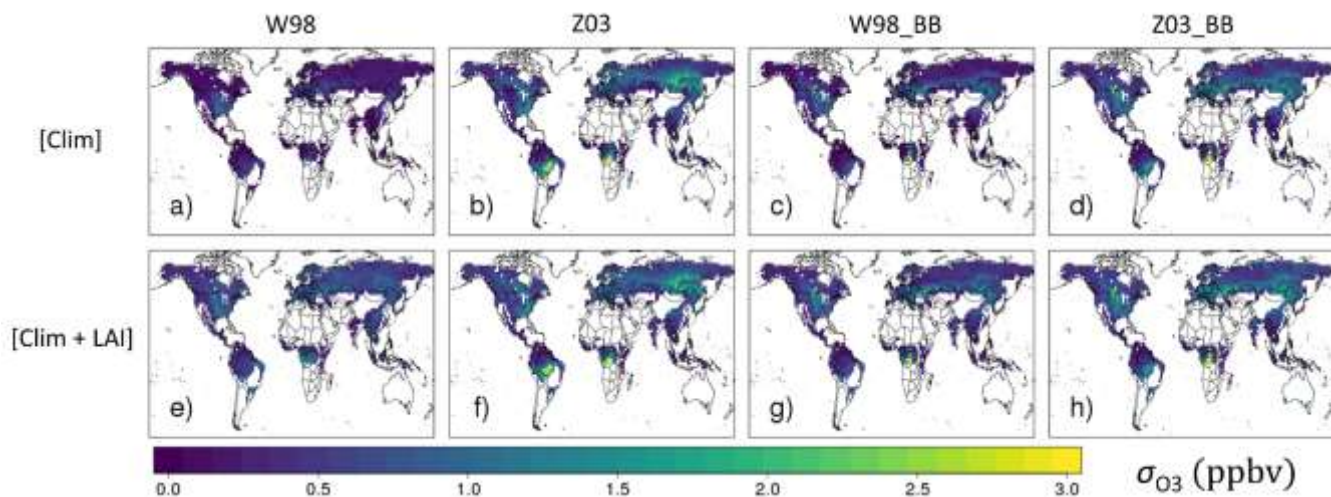
710

711

Figure 10: Interannual coefficient of variation of linearly detrended July mean daytime v_d (CV_{v_d}) during 1982-2011 over

712

vegetated land surface.



713

714 **Figure 11:** Estimated contribution of IAV in July mean daytime v_d to IAV of July mean surface ozone (σ_{O_3}) during 1982-
 715 2011 over vegetated land surface.

716

717

718

719

720

721

722

723

v_d simulation	Meteorology	LAI	Atmospheric CO ₂ concentration
[Clim]	MERRA-2 meteorology	LAI3g monthly climatology	390 ppm
[Clim+LAI]		LAI3g monthly time series	
[Clim+LAI+CO ₂]			Manoa Loa time series

724 **Table 1:** List of v_d simulations with input data

725

Land types	Metrics	Static LAI				Dynamic LAI			
		W98	Z03	W89-BB	Z03_BB	W98	Z03	W89-BB	Z03_BB
Dec (N=8)	<i>NMBF</i>	0.134	-0.367	-0.287	-0.142	0.119	-0.376	-0.299	-0.153
	<i>NMAEF</i>	0.322	0.369	0.305	0.215	0.319	0.376	0.321	0.226
Con	<i>NMBF</i>	-0.362	-0.217	-0.252	-0.025	-0.355	-0.209	-0.248	-0.023

(N=16)	<i>NMAEF</i>	0.448	0.455	0.483	0.399	0.427	0.458	0.470	0.394
Tro	<i>NMBF</i>	0.080	-0.808	-0.086	-0.438	0.075	-0.813	-0.090	-0.441
(N=5)	<i>NMAEF</i>	0.423	0.831	0.404	0.569	0.422	0.832	0.399	0.567
Gra	<i>NMBF</i>	0.276	0.015	0.175	0.097	0.294	0.011	0.186	0.110
(N=10)	<i>NMAEF</i>	0.392	0.479	0.307	0.318	0.396	0.467	0.302	0.311
Cro	<i>NMBF</i>	0.297	0.360	0.241	0.282	0.318	0.371	0.255	0.292
(N=11)	<i>NMAEF</i>	0.473	0.541	0.474	0.570	0.485	0.550	0.480	0.576

726 **Table 2:** Performance metrics (*NMBF* and *NMAEF*) for daytime average v_d simulated by the four dry deposition
727 parameterizations, with N referring to number of data points (1 data points = 1 seasonal mean). “Static LAI” is the result
728 from [Clim] run, which uses 1982-2011 AVHRR monthly climatological LAI, while “Dynamic LAI” is the result from
729 [Clim+LAI], which uses 1982-2011 AVHRR LAI time series. Dec = deciduous forest, Con = coniferous forest, Tro =
730 tropical rainforest, Gra = grassland, Cro = cropland. N indicates the number of observational datasets involved in that
731 particular land type. The best performing parameterization for each land type has its performance metrics bolded.

732
733
734
735
736
737

738 References

- 739 Ainsworth, E. A. and Rogers, A.: The response of photosynthesis and stomatal conductance to rising [CO₂]: Mechanisms and
740 environmental interactions, *Plant, Cell Environ.*, 30(3), 258–270, doi:10.1111/j.1365-3040.2007.01641.x, 2007.
- 741 Ainsworth, E. A., Yendrek, C. R., Sitch, S., Collins, W. J. and Emberson, L. D.: The Effects of Tropospheric Ozone on Net
742 Primary Productivity and Implications for Climate Change, *Annu. Rev. Plant Biol.*, 63(1), 637–661, doi:10.1146/annurev-
743 arplant-042110-103829, 2012.
- 744 Altimir, N., Kolari, P., Tuovinen, J.-P., Vesala, T., Bäck, J., Suni, T., Kulmala, M. and Hari, P.: Foliage surface ozone
745 deposition: a role for surface moisture?, *Biogeosciences Discuss.*, 2, 1739–1793, doi:10.5194/bgd-2-1739-2005, 2006.
- 746 Ashworth, K., Chung, S. H., Griffin, R. J., Chen, J., Forkel, R., Bryan, A. M. and Steiner, A. L.: FORest Canopy Atmosphere
747 Transfer (FORCAsT) 1.0: A 1-D model of biosphere-atmosphere chemical exchange, *Geosci. Model Dev.*, doi:10.5194/gmd-
748 8-3765-2015, 2015.
- 749 Avnery, S., Mauzerall, D. L., Liu, J. and Horowitz, L. W.: Global crop yield reductions due to surface ozone exposure: 1. Year
750 2000 crop production losses and economic damage, *Atmos. Environ.*, 45(13), 2284–2296,

751 doi:10.1016/j.atmosenv.2010.11.045, 2011.

752 Baldocchi, D., Falge, E., Gu, L., Olson, R., Hollinger, D., Running, S., Anthoni, P., Bernhofer, C., Davis, K., Evans, R.,
753 Fuentes, J., Goldstein, A., Katul, G., Law, B., Lee, X., Malhi, Y., Meyers, T., Munger, W., Oechel, W., Paw, U. K. T.,
754 Pilegaard, K., Schmid, H. P., Valentini, R., Verma, S., Vesala, T., Wilson, K. and Wofsy, S.: FLUXNET: A New Tool to
755 Study the Temporal and Spatial Variability of Ecosystem-Scale Carbon Dioxide, Water Vapor, and Energy Flux Densities,
756 Bull. Am. Meteorol. Soc., doi:10.1175/1520-0477(2001)082<2415:FANTTS>2.3.CO;2, 2001.

757 Baldocchi, D. D., Hicks, B. B. and Camara, P.: A canopy stomatal resistance model for gaseous deposition to vegetated
758 surfaces, Atmos. Environ., 21(1), 91–101, doi:10.1016/0004-6981(87)90274-5, 1987.

759 Ball, J. T., Woodrow, I. E. and Berry, J. A.: A Model Predicting Stomatal Conductance and its Contribution to the Control of
760 Photosynthesis under Different Environmental Conditions, in Progress in Photosynthesis Research, pp. 221–224., 1987.

761 Brook, J. R., Zhang, L., Di-Giovanni, F. and Padro, J.: Description and evaluation of a model of deposition velocities for
762 routine estimates of air pollutant dry deposition over North America. Part I: Model development, Atmos. Environ.,
763 doi:10.1016/S1352-2310(99)00250-2, 1999.

764 Brown-Steiner, B., Selin, N. E., Prinn, R. G., Monier, E., Tilmes, S., Emmons, L. and Garcia-Menendez, F.: Maximizing ozone
765 signals among chemical, meteorological, and climatological variability, Atmos. Chem. Phys., doi:10.5194/acp-18-8373-2018,
766 2018.

767 Centoni, F.: Global scale modelling of ozone deposition processes and interaction between surface ozone and climate change
768 A thesis presented for the degree The University of Edinburgh, University of Edinburgh., 2017.

769 Chen, B., Black, T. A., Coops, N. C., Hilker, T., Trofymow, J. A. and Morgenstern, K.: Assessing tower flux footprint
770 climatology and scaling between remotely sensed and eddy covariance measurements, Boundary-Layer Meteorol.,
771 doi:10.1007/s10546-008-9339-1, 2009.

772 Chen, B., Coops, N. C., Fu, D., Margolis, H. A., Amiro, B. D., Black, T. A., Arain, M. A., Barr, A. G., Bourque, C. P. A.,
773 Flanagan, L. B., Lafleur, P. M., McCaughey, J. H. and Wofsy, S. C.: Characterizing spatial representativeness of flux tower
774 eddy-covariance measurements across the Canadian Carbon Program Network using remote sensing and footprint analysis,
775 Remote Sens. Environ., doi:10.1016/j.rse.2012.06.007, 2012.

776 Clifton, O. E., Fiore, A. M., Munger, J. W., Malyshev, S., Horowitz, L. W., Shevliakova, E., Paulot, F., Murray, L. T. and
777 Griffin, K. L.: Interannual variability in ozone removal by a temperate deciduous forest, Geophys. Res. Lett., 44(1), 542–552,
778 doi:10.1002/2016GL070923, 2017.

779 Clifton, O. E., Fiore, A. M., Munger, J. W. and Wehr, R.: Spatiotemporal controls on observed daytime ozone deposition
780 velocity over Northeastern U.S. forests during summer., 2019.

781 Coe, H., Gallagher, M. W., Choularton, T. W. and Dore, C.: Canopy scale measurements of stomatal and cuticular O₃ uptake
782 by sitka spruce, Atmos. Environ., doi:10.1016/1352-2310(95)00034-V, 1995.

783 Collatz, G., Ribas-Carbo, M. and Berry, J.: Coupled Photosynthesis-Stomatal Conductance Model for Leaves of C₄ Plants,
784 Aust. J. Plant Physiol., 19(5), 519, doi:10.1071/PP9920519, 1992.

785 Collatz, G. J., Ball, J. T., Grivet, C. and Berry, J. A.: Physiological and environmental regulation of stomatal conductance,
786 photosynthesis and transpiration: a model that includes a laminar boundary layer, *Agric. For. Meteorol.*, 54(2–4), 107–136,
787 doi:10.1016/0168-1923(91)90002-8, 1991.

788 Coyle, M., Nemitz, E., Storeton-West, R., Fowler, D. and Cape, J. N.: Measurements of ozone deposition to a potato canopy,
789 *Agric. For. Meteorol.*, doi:10.1016/j.agrformet.2008.10.020, 2009.

790 Dai, Y., Shangguan, W., Wei, N., Xin, Q., Yuan, H., Zhang, S. and Liu, S.: SOIL A review of the global soil property maps
791 for Earth system models, , (2016), 137–158, 2019.

792 Droppo, J. G.: Concurrent measurements of ozone dry deposition using eddy correlation and profile flux methods., *J. Geophys.*
793 *Res.*, doi:10.1029/JD090iD01p02111, 1985.

794 Ducker, J. A., Holmes, C. D., Keenan, T. F., Fares, S., Goldstein, A. H., Mammarella, I., William Munger, J. and Schnell, J.:
795 Synthetic ozone deposition and stomatal uptake at flux tower sites, *Biogeosciences*, doi:10.5194/bg-15-5395-2018, 2018.

796 Emberson, L. D., Wieser, G. and Ashmore, M. R.: Modelling of stomatal conductance and ozone flux of Norway spruce:
797 Comparison with field data, in *Environmental Pollution.*, 2000.

798 Fang, H., Li, W. and Myneni, R. B.: The impact of potential land cover misclassification on modis leaf area index (LAI)
799 estimation: A statistical perspective, *Remote Sens.*, doi:10.3390/rs5020830, 2013.

800 Fares, S., McKay, M., Holzinger, R. and Goldstein, A. H.: Ozone fluxes in a *Pinus ponderosa* ecosystem are dominated by
801 non-stomatal processes: Evidence from long-term continuous measurements, *Agric. For. Meteorol.*, 150(3), 420–431,
802 doi:10.1016/j.agrformet.2010.01.007, 2010.

803 Fares, S., Savi, F., Muller, J., Matteucci, G. and Paoletti, E.: Simultaneous measurements of above and below canopy ozone
804 fluxes help partitioning ozone deposition between its various sinks in a Mediterranean Oak Forest, *Agric. For. Meteorol.*, 198,
805 181–191, doi:10.1016/j.agrformet.2014.08.014, 2014.

806 Fares, S., Conte, A. and Chabbi, A.: Ozone flux in plant ecosystems: new opportunities for long-term monitoring networks to
807 deliver ozone-risk assessments, *Environ. Sci. Pollut. Res.*, 1–9, doi:10.1007/s11356-017-0352-0, 2017.

808 Farquhar, G. D., Von Caemmerer, S. and Berry, J. A.: A Biochemical Model of Photosynthetic CO₂ Assimilation in Leaves
809 of C₃ Species, *Planta*, 149, 78–90, doi:10.1007/BF00386231, 1980.

810 Finkelstein, P. L., Ellestad, T. G., Clarke, J. F., Meyers, T. P., Schwede, D. B., Hebert, E. O. and Neal, J. A.: Ozone and sulfur
811 dioxide dry deposition to forests: Observations and model evaluation, *J. Geophys. Res. Atmos.*, doi:10.1029/2000JD900185,
812 2000.

813 Fiore, A. M., Oberman, J. T., Lin, M. Y., Zhang, L., Clifton, O. E., Jacob, D. J., Naik, V., Horowitz, L. W., Pinto, J. P. and
814 Milly, G. P.: Estimating North American background ozone in U.S. surface air with two independent global models:
815 Variability, uncertainties, and recommendations, *Atmos. Environ.*, doi:10.1016/j.atmosenv.2014.07.045, 2014.

816 Foken, T.: 50 years of the Monin-Obukhov similarity theory, *Boundary-Layer Meteorol.*, doi:10.1007/s10546-006-9048-6,
817 2006.

818 Fowler, D., Flechard, C., Cape, J. N., Storeton-West, R. L. and Coyle, M.: Measurements of ozone deposition to vegetation

819 quantifying the flux, the stomatal and non-stomatal components, *Water, Air, Soil Pollut.*, doi:10.1023/A:1012243317471,
820 2001.

821 Fowler, D., Nemitz, E., Misztal, P., di Marco, C., Skiba, U., Ryder, J., Helfter, C., Neil Cape, J., Owen, S., Dorsey, J.,
822 Gallagher, M. W., Coyle, M., Phillips, G., Davison, B., Langford, B., MacKenzie, R., Muller, J., Siong, J., Dari-Salisburgo,
823 C., di Carlo, P., Aruffo, E., Giammaria, F., Pyle, J. A. and Nicholas Hewitt, C.: Effects of land use on surface-atmosphere
824 exchanges of trace gases and energy in Borneo: Comparing fluxes over oil palm plantations and a rainforest, *Philos. Trans. R.*
825 *Soc. B Biol. Sci.*, doi:10.1098/rstb.2011.0055, 2011.

826 Franks, P. J., Adams, M. A., Amthor, J. S., Barbour, M. M., Berry, J. A., Ellsworth, D. S., Farquhar, G. D., Ghannoum, O.,
827 Lloyd, J., McDowell, N., Norby, R. J., Tissue, D. T. and von Caemmerer, S.: Sensitivity of plants to changing atmospheric
828 CO₂ concentration: From the geological past to the next century, *New Phytol.*, 197(4), 1077–1094, doi:10.1111/nph.12104,
829 2013.

830 Fu, Y. and Tai, A. P. K.: Impact of climate and land cover changes on tropospheric ozone air quality and public health in East
831 Asia between 1980 and 2010, *Atmos. Chem. Phys.*, 15(17), 10093–10106, doi:10.5194/acp-15-10093-2015, 2015.

832 Ganzeveld, L., Bouwman, L., Stehfest, E., van Vuuren, D. P., Eickhout, B. and Lelieveld, J.: Impact of future land use and
833 land cover changes on atmospheric chemistry-climate interactions, *J. Geophys. Res.*, 115(D23), D23301,
834 doi:10.1029/2010JD014041, 2010.

835 Gao, W. and Wesely, M. L.: Modeling gaseous dry deposition over regional scales with satellite observations-I. Model
836 development, *Atmos. Environ.*, 29(6), 727–737, doi:10.1016/1352-2310(94)00284-R, 1995.

837 Geddes, J. A. and Martin, R. V.: Global deposition of total reactive nitrogen oxides from 1996 to 2014 constrained with satellite
838 observations of NO₂ columns, *Atmos. Chem. Phys.*, doi:10.5194/acp-17-10071-2017, 2017.

839 Geddes, J. A., Heald, C. L., Silva, S. J. and Martin, R. V.: Land cover change impacts on atmospheric chemistry: Simulating
840 projected large-scale tree mortality in the United States, *Atmos. Chem. Phys.*, 16(4), 2323–2340, doi:10.5194/acp-16-2323-
841 2016, 2016.

842 Gelaro, R., McCarty, W., Suárez, M. J., Todling, R., Molod, A., Takacs, L., Randles, C. A., Darmenov, A., Bosilovich, M. G.,
843 Reichle, R., Wargan, K., Coy, L., Cullather, R., Draper, C., Akella, S., Buchard, V., Conaty, A., da Silva, A. M., Gu, W., Kim,
844 G. K., Koster, R., Lucchesi, R., Merkova, D., Nielsen, J. E., Partyka, G., Pawson, S., Putman, W., Rienecker, M., Schubert, S.
845 D., Sienkiewicz, M. and Zhao, B.: The modern-era retrospective analysis for research and applications, version 2 (MERRA-
846 2), *J. Clim.*, 30(14), 5419–5454, doi:10.1175/JCLI-D-16-0758.1, 2017.

847 Gerosa, G., Vitale, M., Finco, A., Manes, F., Denti, A. B. and Cieslik, S.: Ozone uptake by an evergreen Mediterranean Forest
848 (*Quercus ilex*) in Italy. Part I: Micrometeorological flux measurements and flux partitioning, *Atmos. Environ.*, 39(18), 3255–
849 3266, doi:10.1016/j.atmosenv.2005.01.056, 2005.

850 Gerosa, G., Marzuoli, R., Monteleone, B., Chiesa, M. and Finco, A.: Vertical ozone gradients above forests. Comparison of
851 different calculation options with direct ozone measurements above a mature forest and consequences for ozone risk
852 assessment, *Forests*, 8(9), doi:10.3390/f8090337, 2017.

853 Hardacre, C., Wild, O. and Emberson, L.: An evaluation of ozone dry deposition in global scale chemistry climate models,
854 *Atmos. Chem. Phys.*, 15(11), 6419–6436, doi:10.5194/acp-15-6419-2015, 2015.

855 Heald, C. L. and Geddes, J. A.: The impact of historical land use change from 1850 to 2000 on secondary particulate matter
856 and ozone, *Atmos. Chem. Phys.*, doi:10.5194/acp-16-14997-2016, 2016.

857 Hole, L. R., Semb, A. and Tørseth, K.: Ozone deposition to a temperate coniferous forest in Norway; gradient method
858 measurements and comparison with the EMEP deposition module, in *Atmospheric Environment.*, 2004.

859 Hollaway, M. J., Arnold, S. R., Collins, W. J., Folberth, G. and Rap, A.: Sensitivity of midnineteenth century tropospheric
860 ozone to atmospheric chemistry-vegetation interactions, *J. Geophys. Res. Atmos.*, 122(4), 2452–2473,
861 doi:10.1002/2016JD025462, 2017.

862 Hoshika, Y., Carriero, G., Feng, Z., Zhang, Y. and Paoletti, E.: Determinants of stomatal sluggishness in ozone-exposed
863 deciduous tree species, *Sci. Total Environ.*, 481(1), 453–458, doi:10.1016/j.scitotenv.2014.02.080, 2014.

864 Hu, L., Jacob, D. J., Liu, X., Zhang, Y., Zhang, L., Kim, P. S., Sulprizio, M. P. and Yantosca, R. M.: Global budget of
865 tropospheric ozone: Evaluating recent model advances with satellite (OMI), aircraft (IAGOS), and ozonesonde observations,
866 *Atmos. Environ.*, 167, 323–334, doi:10.1016/j.atmosenv.2017.08.036, 2017.

867 Huang, L., McDonald-Buller, E. C., McGaughey, G., Kimura, Y. and Allen, D. T.: The impact of drought on ozone dry
868 deposition over eastern Texas, *Atmos. Environ.*, 127, 176–186, doi:10.1016/j.atmosenv.2015.12.022, 2016.

869 Jacob, D. J. and Wofsy, S. C.: Budgets of Reactive Nitrogen, Hydrocarbons, and Ozone Over the Amazon Forest during the
870 Wet Season, *J. Geophys. Res.*, 95, 16737–16754, doi:10.1029/JD095iD10p16737, 1990.

871 Jacob, D. J., Fan, S.-M., Wofsy, S. C., Spiro, P. A., Bakwin, P. S., Ritter, J. A., Browell, E. V., Gregory, G. L., Fitzjarrald, D.
872 R. and Moore, K. E.: Deposition of ozone to tundra, *J. Geophys. Res.*, doi:10.1029/91JD02696, 1992.

873 Jarvis, P. G.: The Interpretation of the Variations in Leaf Water Potential and Stomatal Conductance Found in Canopies in the
874 Field, *Philos. Trans. R. Soc. B Biol. Sci.*, 273(927), 593–610, doi:10.1098/rstb.1976.0035, 1976.

875 Jerrett, M., Burnett, R. T., Pope, C. A., Ito, K., Thurston, G., Krewski, D., Shi, Y., Calle, E. and Thun, M.: Long-Term Ozone
876 Exposure and Mortality, *N. Engl. J. Med.*, 360(11), 1085–1095, doi:10.1056/NEJMoa0803894, 2009.

877 Jiang, C., Ryu, Y., Fang, H., Myneni, R., Claverie, M. and Zhu, Z.: Inconsistencies of interannual variability and trends in
878 long-term satellite leaf area index products, *Glob. Chang. Biol.*, doi:10.1111/gcb.13787, 2017.

879 Junninen, H., Lauri, A., Keronen, P., Aalto, P., Hiltunen, V., Hari, P. and Kulmala, M.: Smart-SMEAR: On-line data
880 exploration and visualization tool for SMEAR stations, *Boreal Environ. Res.*, 14(4), 447–457, 2009.

881 Kattge, J. and Knorr, W.: Temperature acclimation in a biochemical model of photosynthesis: A reanalysis of data from 36
882 species, *Plant, Cell Environ.*, 30(9), 1176–1190, doi:10.1111/j.1365-3040.2007.01690.x, 2007.

883 Kavassalis, S. C. and Murphy, J. G.: Understanding ozone-meteorology correlations: A role for dry deposition, *Geophys. Res.
884 Lett.*, 44(6), 2922–2931, doi:10.1002/2016GL071791, 2017.

885 Keeling, C. D., Stephen, C., Piper, S. C., Bacastow, R. B., Wahlen, M., Whorf, T. P., Heimann, M. and Meijer, H. a.: Exchanges
886 of atmospheric CO₂ and ¹³CO₂ with the terrestrial biosphere and oceans from 1978 to 2000, *Glob. Asp. SIO Ref. Ser. Scripps*

887 Inst. Ocean. San Diego, doi:10.1007/b138533, 2001.

888 Keronen, P., Reissell, a, Rannik, Ü., Pohja, T., Siivola, E., Hiltunen, V., Hari, P., Kulmala, M. and Vesala, T.: Ozone flux
889 measurements over a Scots pine forest using eddy covariance method: Performance evaluation and comparison with flux-
890 profile method, *Boreal Environ. Res.*, 8(4), 425–443 [online] Available from:
891 [http://www.scopus.com/inward/record.url?eid=2-s2.0-](http://www.scopus.com/inward/record.url?eid=2-s2.0-0347884158&partnerID=40&md5=4ad114fb52c557d36cc8a0ec1ab8bb7e)
892 [0347884158&partnerID=40&md5=4ad114fb52c557d36cc8a0ec1ab8bb7e](http://www.scopus.com/inward/record.url?eid=2-s2.0-0347884158&partnerID=40&md5=4ad114fb52c557d36cc8a0ec1ab8bb7e), 2003.

893 Kharol, S. K., Shephard, M. W., Mclinden, C. A., Zhang, L., Sioris, C. E., O'Brien, J. M., Vet, R., Cady-Pereira, K. E., Hare,
894 E., Siemons, J. and Krotkov, N. A.: Dry Deposition of Reactive Nitrogen From Satellite Observations of Ammonia and
895 Nitrogen Dioxide Over North America, *Geophys. Res. Lett.*, doi:10.1002/2017GL075832, 2018.

896 Kurpius, M. R., McKay, M. and Goldstein, A. H.: Annual ozone deposition to a Sierra Nevada ponderosa pine plantation,
897 *Atmos. Environ.*, doi:10.1016/S1352-2310(02)00423-5, 2002.

898 Lamaud, E., Brunet, Y., Labatut, A., Lopez, A., Fontan, J. and Druilhet, A.: The Landes experiment: Biosphere-atmosphere
899 exchanges of ozone and aerosol particles above a pine forest, *J. Geophys. Res.*, doi:10.1029/94JD00668, 1994.

900 Lamaud, E., Carrara, A., Brunet, Y., Lopez, A. and Druilhet, A.: Ozone fluxes above and within a pine forest canopy in dry
901 and wet conditions, *Atmos. Environ.*, 36(1), 77–88, doi:10.1016/S1352-2310(01)00468-X, 2002.

902 Lawrence, P. J. and Chase, T. N.: Representing a new MODIS consistent land surface in the Community Land Model (CLM
903 3.0), *J. Geophys. Res. Biogeosciences*, 112(1), doi:10.1029/2006JG000168, 2007.

904 Li, D., Bou-Zeid, E., Barlage, M., Chen, F. and Smith, J. A.: Development and evaluation of a mosaic approach in the WRF-
905 Noah framework, *J. Geophys. Res. Atmos.*, 118(21), 11918–11935, doi:10.1002/2013JD020657, 2013.

906 Lin, Y., Medlyn, B. and Duursma, R.: Optimal stomatal behaviour around the world, *Nat. Clim. ...*, (March), 1–6,
907 doi:10.1038/NCLIMATE2550, 2015.

908 Lin, M., Malyshev, S., Shevliakova, E., Paulot, F., Horowitz, L. W., Fares, S., Mikkelsen, T. N. and Zhang, L.: Sensitivity of
909 ozone dry deposition to ecosystem-atmosphere interactions: A critical appraisal of observations and simulations, *Global*
910 *Biogeochemical Cycles*, 3, doi: 10.1029/2018GB006157.

911 Lombardozzi, D., Sparks, J. P., Bonan, G. and Levis, S.: Ozone exposure causes a decoupling of conductance and
912 photosynthesis: Implications for the Ball-Berry stomatal conductance model, *Oecologia*, 169(3), 651–659,
913 doi:10.1007/s00442-011-2242-3, 2012.

914 Lombardozzi, D., Levis, S., Bonan, G., Hess, P. G. and Sparks, J. P.: The influence of chronic ozone exposure on global carbon
915 and water cycles, *J. Clim.*, 28(1), 292–305, doi:10.1175/JCLI-D-14-00223.1, 2015.

916 Malhi, Y., Roberts, J. T., Betts, R. A., Killeen, T. J., Li, W. and Nobre, C. A.: Climate change, deforestation, and the fate of
917 the Amazon, *Science* (80-.), doi:10.1126/science.1146961, 2008.

918 Mao, J., Paulot, F., Jacob, D. J., Cohen, R. C., Crounse, J. D., Wennberg, P. O., Keller, C. A., Hudman, R. C., Barkley, M. P.
919 and Horowitz, L. W.: Ozone and organic nitrates over the eastern United States: Sensitivity to isoprene chemistry, *J. Geophys.*
920 *Res. Atmos.*, 118(19), 11256–11268, doi:10.1002/jgrd.50817, 2013.

921 Matsuda, K., Watanabe, I., Wingpud, V., Theramongkol, P., Khummongkol, P., Wangwongwatana, S. and Totsuka, T.: Ozone
922 dry deposition above a tropical forest in the dry season in northern Thailand, *Atmos. Environ.*, 39(14), 2571–2577,
923 doi:10.1016/j.atmosenv.2005.01.011, 2005.

924 McGrath, J. M., Betzelberger, A. M., Wang, S., Shook, E., Zhu, X.-G., Long, S. P. and Ainsworth, E. A.: An analysis of ozone
925 damage to historical maize and soybean yields in the United States, *Proc. Natl. Acad. Sci.*, 112(46), 14390–14395,
926 doi:10.1073/pnas.1509777112, 2015.

927 Mészáros, R., Horváth, L., Weidinger, T., Neftel, A., Nemitz, E., Dammgen, U., Cellier, P. and Loubet, B.: Measurement and
928 modelling ozone fluxes over a cut and fertilized grassland, *Biogeosciences*, doi:10.1029/2002GL016785

929 Meyers, T. P., Finkelstein, P., Clarke, J., Ellestad, T. G. and Sims, P. F.: A multilayer model for inferring dry deposition using
930 standard meteorological measurements, *J. Geophys. Res.*, 103(98), 22645, doi:10.1029/98JD01564, 1998.

931 Mikkelsen, T. N., Ro-Poulsen, H., Hovmand, M. F., Jensen, N. O., Pilegaard, K. and Egeløv, A. H.: Five-year measurements
932 of ozone fluxes to a Danish Norway spruce canopy, in *Atmospheric Environment.*, 2004.

933 Muller, J. B. A., Percival, C. J., Gallagher, M. W., Fowler, D., Coyle, M. and Nemitz, E.: Sources of uncertainty in eddy
934 covariance ozone flux measurements made by dry chemiluminescence fast response analysers, *Atmos. Meas. Tech.*,
935 doi:10.5194/amt-3-163-2010, 2010.

936 Munger, J. W., Wofsy, S. C., Bakwin, P. S., Fan, S.-M., Goulden, M. L., Daube, B. C., Goldstein, A. H., Moore, K. E. and
937 Fitzjarrald, D. R.: Atmospheric deposition of reactive nitrogen oxides and ozone in a temperate deciduous forest and a subarctic
938 woodland 1. Measurements and mechanisms, *J. Geophys. Res.*, 101657(20), 639–12, doi:10.1029/96JD00230, 1996.

939 Myneni, R. B., Hoffman, S., Knyazikhin, Y., Privette, J. L., Glassy, J., Tian, Y., Wang, Y., Song, X., Zhang, Y., Smith, G. R.,
940 Lotsch, A., Friedl, M., Morisette, J. T., Votava, P., Nemani, R. R. and Running, S. W.: Global products of vegetation leaf area
941 and fraction absorbed PAR from year one of MODIS data, *Remote Sens. Environ.*, 83(1–2), 214–231, doi:10.1016/S0034-
942 4257(02)00074-3, 2002.

943 Norby, R. J. and Zak, D. R.: Ecological Lessons from Free-Air CO₂ Enrichment (FACE) Experiments, *Annu. Rev. Ecol. Evol.*
944 *Syst.*, doi:10.1146/annurev-ecolsys-102209-144647, 2011.

945 Nowlan, C. R., Martin, R. V., Philip, S., Lamsal, L. N., Krotkov, N. A., Marais, E. A., Wang, S. and Zhang, Q.: Global dry
946 deposition of nitrogen dioxide and sulfur dioxide inferred from space-based measurements, *Global Biogeochem. Cycles*,
947 doi:10.1002/2014GB004805, 2014.

948 Oleson, K. W., Lawrence, D. M., Bonan, G. B., Drewniak, B., Huang, M., Koven, C. D., Levis, S., Li, F., Riley, J., Subin, Z.
949 M., Swenson, S. C., Thornton, P. E., Bozbiyik, A., Fisher, R. A., Heald, C. L., Kluzek, E., Lamarque, J.-F., Lawrence, P. J.,
950 Leung, L. R., Lipscomb, W., Muszala, S., Ricciuto, D. M., Sacks, W. J., Sun, Y., Tang, J. and Yang, Z.-L.: Technical
951 Description of version 4.5 of the Community Land Model (CLM)., 2013.

952 Olson, D. M., Dinerstein, E., Wikramanayake, E. D., Burgess, N. D., Powell, G. V. N., Underwood, E. C., D’amico, J. A.,
953 Itoua, I., Strand, H. E., Morrison, J. C., Loucks, C. J., Allnutt, T. F., Ricketts, T. H., Kura, Y., Lamoreux, J. F., Wettengel, W.
954 W., Hedao, P. and Kassem, K. R.: Terrestrial Ecoregions of the World: A New Map of Life on Earth, *Bioscience*,

955 doi:10.1641/0006-3568(2001)051[0933:TEOTWA]2.0.CO;2, 2001.

956 Padro, J., den Hartog, G. and Neumann, H. H.: An investigation of the ADOM dry deposition module using summertime
957 O₃ measurements above a deciduous forest, *Atmos. Environ. Part A, Gen. Top.*, doi:10.1016/0960-1686(91)90027-5, 1991.

958 Padro, J., Massman, W. J., Shaw, R. H., Delany, A. and Oncley, S. P.: A comparison of some aerodynamic resistance methods
959 using measurements over cotton and grass from the 1991 California ozone deposition experiment, *Boundary-Layer Meteorol.*,
960 doi:10.1007/BF00712174, 1994.

961 Paulson, C. A.: The Mathematical Representation of Wind Speed and Temperature Profiles in the Unstable Atmospheric
962 Surface Layer, *J. Appl. Meteorol.*, doi:10.1175/1520-0450(1970)009<0857:tmrows>2.0.co;2, 2002.

963 Pilegaard, K., Hummelshøj, P. and Jensen, N. O.: Fluxes of ozone and nitrogen dioxide measured by eddy correlation over a
964 harvested wheat field, *Atmos. Environ.*, doi:10.1016/S1352-2310(97)00194-5, 1998.

965 Pio, C. ., Feliciano, M. ., Vermeulen, A. . and Sousa, E. .: Seasonal variability of ozone dry deposition under southern European
966 climate conditions, in Portugal, *Atmos. Environ.*, doi:10.1016/S1352-2310(99)00276-9, 2000.

967 Pleim, J. and Ran, L.: Surface flux modeling for air quality applications, *Atmosphere (Basel)*., 2(3), 271–302,
968 doi:10.3390/atmos2030271, 2011.

969 Potier, E., Ogée, J., Jouanguy, J., Lamaud, E., Stella, P., Personne, E., Durand, B., Mascher, N. and Loubet, B.: Multilayer
970 modelling of ozone fluxes on winter wheat reveals large deposition on wet senescing leaves, *Agric. For. Meteorol.*, 211–212,
971 58–71, doi:10.1016/j.agrformet.2015.05.006, 2015.

972 Potier, E., Loubet, B., Durand, B., Flura, D., Bourdat-Deschamps, M., Ciuraru, R. and Ogée, J.: Chemical reaction rates of
973 ozone in water infusions of wheat, beech, oak and pine leaves of different ages, *Atmos. Environ.*, 151, 176–187,
974 doi:10.1016/j.atmosenv.2016.11.069, 2017.

975 R core team: R: A language and environment for statistical computing., R Found. Stat. Comput. Vienna, Austria.,
976 doi:http://www.R-project.org/, 2017.

977 Ran, L., Pleim, J., Song, C., Band, L., Walker, J. T. and Binkowski, F. S.: A photosynthesis-based two-leaf canopy stomatal
978 conductance model for meteorology and air quality modeling with WRF/CMAQ PX LSM, *J. Geophys. Res.*, 122(3), 1930–
979 1952, doi:10.1002/2016JD025583, 2017a.

980 Ran, L., Pleim, J., Song, C., Band, L., Walker, J. T. and Binkowski, F. S.: A photosynthesis-based two-leaf canopy stomatal
981 conductance model for meteorology and air quality modeling with WRF/CMAQ PX LSM, *J. Geophys. Res.*, 122(3), 1930–
982 1952, doi:10.1002/2016JD025583, 2017b.

983 Rannik, Ü., Altimir, N., Mammarella, I., Bäck, J., Rinne, J., Ruuskanen, T. M., Hari, P., Vesala, T. and Kulmala, M.: Ozone
984 deposition into a boreal forest over a decade of observations: Evaluating deposition partitioning and driving variables, *Atmos.*
985 *Chem. Phys.*, 12(24), 12165–12182, doi:10.5194/acp-12-12165-2012, 2012.

986 Reich, P. B.: Quantifying plant response to ozone: a unifying theory, *Tree Physiol.*, 3(0), 63–91, doi:10.1093/treephys/3.1.63,
987 1987.

988 Rienecker, M. M. and Coauthors: The GEOS-5 Data Assimilation System—Documentation of versions 5.0.1 and 5.1.0, and

989 5.2.0, NASA Tech. Rep. Ser. Glob. Model. Data Assim. NASA/TM-2008-104606, doi:10.2759/32049, 2008.

990 Rigden, A. J. and Salvucci, G. D.: Stomatal response to humidity and CO₂ implicated in recent decline in US evaporation,
991 Glob. Chang. Biol., doi:10.1111/gcb.13439, 2017.

992 Rummel, U., Ammann, C., Kirkman, G. A., Moura, M. A. L., Foken, T., Andreae, M. O. and Meixner, F. X.: Seasonal variation
993 of ozone deposition to a tropical rain forest in southwest Amazonia, Atmos. Chem. Phys., doi:10.5194/acp-7-5415-2007, 2007.

994 Sadiq, M., Tai, A. P. K., Lombardozzi, D. and Val Martin, M.: Effects of ozone-vegetation coupling on surface ozone air
995 quality via biogeochemical and meteorological feedbacks, Atmos. Chem. Phys., 17(4), 3055–3066, doi:10.5194/acp-17-3055-
996 2017, 2017.

997 Sanderson, M. G., Collins, W. J., Hemming, D. L. and Betts, R. A.: Stomatal conductance changes due to increasing carbon
998 dioxide levels: Projected impact on surface ozone levels, Tellus, Ser. B Chem. Phys. Meteorol., 59(3), 404–411,
999 doi:10.1111/j.1600-0889.2007.00277.x, 2007.

1000 Sen, P. K.: Estimates of the Regression Coefficient Based on Kendall's Tau, J. Am. Stat. Assoc.,
1001 doi:10.1080/01621459.1968.10480934, 1968.

1002 Silva, S. J. and Heald, C. L.: Investigating Dry Deposition of Ozone to Vegetation, J. Geophys. Res. Atmos., 123(1), 559–573,
1003 doi:10.1002/2017JD027278, 2018.

1004 Simpson, D., Benedictow, A., Berge, H., Bergström, R., Emberson, L. D., Fagerli, H., Flechard, C. R., Hayman, G. D., Gauss,
1005 M., Jonson, J. E., Jenkin, M. E., Nyíri, A., Richter, C., Semeena, V. S., Tsyro, S., Tuovinen, J.-P., Valdebenito, A. and Wind,
1006 P.: The EMEP MSC-W chemical transport model – technical description, Atmos. Chem. Phys. Atmos. Chem. Phys., 12, 7825–
1007 7865, doi:10.5194/acp-12-7825-2012, 2012.

1008 Sitch, S., Cox, P. M., Collins, W. J. and Huntingford, C.: Indirect radiative forcing of climate change through ozone effects on
1009 the land-carbon sink, Nature, 448(7155), 791–794, doi:10.1038/nature06059, 2007.

1010 Song-Miao, F., Wofsy, S. C., Bakwin, P. S., Jacob, D. J. and Fitzjarrald, D. R.: Atmosphere-biosphere exchange of CO₂ and
1011 O₃ in the central Amazon forest, J. Geophys. Res., doi:10.1029/JD095iD10p16851, 1990.

1012 Stella, P., Personne, E., Loubet, B., Lamaud, E., Ceschia, E., B^{??}ziat, P., Bonnefond, J. M., Irvine, M., Keravec, P., Mascher,
1013 N. and Cellier, P.: Predicting and partitioning ozone fluxes to maize crops from sowing to harvest: The Surf_{atm}-O₃ model,
1014 Biogeosciences, 8(10), 2869–2886, doi:10.5194/bg-8-2869-2011, 2011.

1015 Stocker, D. W., Stedman, D. H., Zeller, K. F., Massman, W. J. and Fox, D. G.: Fluxes of nitrogen oxides and ozone measured
1016 by eddy correlation over a shortgrass prairie, J. Geophys. Res., doi:10.1029/93JD00871, 1993.

1017 Sun, S., Moravek, A., Trebs, I., Kesselmeier, J. and Sörgel, M.: Investigation of the influence of liquid surface films on O₃
1018 and PAN deposition to plant leaves coated with organic/inorganic solution, J. Geophys. Res. Atmos., 121(23), 14,239-14,256,
1019 doi:10.1002/2016JD025519, 2016.

1020 Sun, Y., Gu, L. and Dickinson, R. E.: A numerical issue in calculating the coupled carbon and water fluxes in a climate model,
1021 J. Geophys. Res. Atmos., doi:10.1029/2012JD018059, 2012.

1022 Tai, A. P. K., Martin, M. V. and Heald, C. L.: Threat to future global food security from climate change and ozone air pollution,

1023 Nat. Clim. Chang., 4(9), 817–821, doi:10.1038/nclimate2317, 2014.

1024 Travis, K. R., Jacob, D. J., Fisher, J. A., Kim, P. S., Marais, E. A., Zhu, L., Yu, K., Miller, C. C., Yantosca, R. M., Sulprizio,
1025 M. P., Thompson, A. M., Wennberg, P. O., Crounse, J. D., St Clair, J. M., Cohen, R. C., Laughner, J. L., Dibb, J. E., Hall, S.
1026 R., Ullmann, K., Wolfe, G. M., Pollack, I. B., Peischl, J., Neuman, J. A. and Zhou, X.: Why do models overestimate surface
1027 ozone in the Southeast United States?, *Atmos. Chem. Phys.*, 16(21), 13561–13577, doi:10.5194/acp-16-13561-2016, 2016.

1028 Turnipseed, A. A., Burns, S. P., Moore, D. J. P., Hu, J., Guenther, A. B. and Monson, R. K.: Controls over ozone deposition
1029 to a high elevation subalpine forest, *Agric. For. Meteorol.*, doi:10.1016/j.agrformet.2009.04.001, 2009.

1030 Val Martin, M., Heald, C. L. and Arnold, S. R.: Coupling dry deposition to vegetation phenology in the {Community} {Earth}
1031 {System} {Model}: {Implications} for the simulation of surface {O} ₃, *Geophys. Res. Lett.*, 41(8), 2988–2996,
1032 doi:10.1002/2014GL059651, 2014.

1033 Wang, Y., Jacob, D. J. and Logan, J. A.: Global simulation of tropospheric O₃-NO_x-hydrocarbon chemistry: 1. Model
1034 formulation, *J. Geophys. Res. Atmos.*, 103(D9), 10713–10725, doi:10.1029/98JD00158, 1998.

1035 Wesely, M. L.: Parameterization of surface resistances to gaseous dry deposition in regional-scale numerical models, *Atmos.*
1036 *Environ.*, 41(SUPPL.), 52–63, doi:10.1016/j.atmosenv.2007.10.058, 1989.

1037 Wesely, M. L. and Hicks, B. B.: Some Factors that Affect the Deposition Rates of Sulfur Dioxide and Similar Gases on
1038 Vegetation, *J. Air Pollut. Control Assoc.*, 27(11), 1110–1116, doi:10.1080/00022470.1977.10470534, 1977.

1039 Wesely, M. L. and Hicks, B. B.: A review of the current status of knowledge on dry deposition, *Atmos. Environ.*, 34(12–14),
1040 2261–2282, doi:10.1016/S1352-2310(99)00467-7, 2000.

1041 Wild, O.: Modelling the global tropospheric ozone budget: exploring the variability in current models, *Atmos. Chem. Phys.*,
1042 7(10), 2643–2660, doi:10.5194/acp-7-2643-2007, 2007.

1043 Wittig, V. E., Ainsworth, E. A. and Long, S. P.: To what extent do current and projected increases in surface ozone affect
1044 photosynthesis and stomatal conductance of trees? A meta-analytic review of the last 3 decades of experiments, *Plant, Cell*
1045 *Environ.*, 30(9), 1150–1162, doi:10.1111/j.1365-3040.2007.01717.x, 2007.

1046 Wolfe, G. M., Thornton, J. A., McKay, M. and Goldstein, A. H.: Forest-atmosphere exchange of ozone: Sensitivity to very
1047 reactive biogenic VOC emissions and implications for in-canopy photochemistry, *Atmos. Chem. Phys.*, doi:10.5194/acp-11-
1048 7875-2011, 2011.

1049 Wong, A. Y. H., Tai, A. P. K. and Ip, Y.-Y.: Attribution and Statistical Parameterization of the Sensitivity of Surface Ozone
1050 to Changes in Leaf Area Index Based On a Chemical Transport Model, *J. Geophys. Res. Atmos.*, 1–16,
1051 doi:10.1002/2017JD027311, 2018.

1052 Wu, S., Mickley, L. J., Kaplan, J. O. and Jacob, D. J.: Impacts of changes in land use and land cover on atmospheric chemistry
1053 and air quality over the 21st century, *Atmos. Chem. Phys.*, 12(3), 1597–1609, doi:10.5194/acp-12-1597-2012, 2012.

1054 Wu, Z., Wang, X., Chen, F., Turnipseed, A. A., Guenther, A. B., Niyogi, D., Charusombat, U., Xia, B., William Munger, J.
1055 and Alapaty, K.: Evaluating the calculated dry deposition velocities of reactive nitrogen oxides and ozone from two community
1056 models over a temperate deciduous forest, *Atmos. Environ.*, 45(16), 2663–2674, doi:10.1016/j.atmosenv.2011.02.063, 2011.

1057 Wu, Z., Staebler, R., Vet, R. and Zhang, L.: Dry deposition of O₃ and SO₂ estimated from gradient measurements above a
1058 temperate mixed forest, *Environ. Pollut.*, 210, 202–210, doi:10.1016/j.envpol.2015.11.052, 2016.

1059 Wu, Z., Schwede, D. B., Vet, R., Walker, J. T., Shaw, M., Staebler, R. and Zhang, L.: Evaluation and intercomparison of five
1060 North American dry deposition algorithms at a mixed forest site, *J. Adv. Model. Earth Syst.*, 1–16,
1061 doi:10.1029/2017MS001231, 2018.

1062 Wu, Z. Y., Zhang, L., Wang, X. M. and Munger, J. W.: A modified micrometeorological gradient method for estimating
1063 O₃ dry depositions over a forest canopy, *Atmos. Chem. Phys.*, 15(13), 7487–7496, doi:10.5194/acp-
1064 15-7487-2015, 2015.

1065 Young, P. J., Archibald, A. T., Bowman, K. W., Lamarque, J.-F., Naik, V., Stevenson, D. S., Tilmes, S., Voulgarakis, A.,
1066 Wild, O., Bergmann, D., Cameron-Smith, P., Cionni, I., Collins, W. J., Dalsøren, S. B., Doherty, R. M., Eyring, V., Faluvegi,
1067 G., Horowitz, L. W., Josse, B., Lee, Y. H., MacKenzie, I. A., Nagashima, T., Plummer, D. A., Righi, M., Rumbold, S. T.,
1068 Skeie, R. B., Shindell, D. T., Strode, S. A., Sudo, K., Szopa, S. and Zeng, G.: Pre-industrial to end 21st century projections of
1069 tropospheric ozone from the Atmospheric Chemistry and Climate Model Intercomparison Project (ACCMIP), *Atmos. Chem.*
1070 *Phys.*, doi:10.5194/acp-13-2063-2013, 2013.

1071 Yu, S., Eder, B., Dennis, R., Chu, S.-H. and Schwartz, S. E.: New unbiased symmetric metrics for evaluation of air quality
1072 models, *Atmos. Sci. Lett.*, doi:10.1002/asl.125, 2006.

1073 Zhang, L., Moran, M. D. and Brook, J. R.: A comparison of models to estimate in-canopy photosynthetically active radiation
1074 and their influence on canopy stomatal resistance, *Atmos. Environ.*, doi:10.1016/S1352-2310(01)00225-4, 2001.

1075 Zhang, L., Brook, J. R. and Vet, R.: On ozone dry deposition - With emphasis on non-stomatal uptake and wet canopies,
1076 *Atmos. Environ.*, 36(30), 4787–4799, doi:10.1016/S1352-2310(02)00567-8, 2002.

1077 Zhang, L., Brook, J. R. and Vet, R.: A revised parameterization for gaseous dry deposition in air-quality models, *Atmos. Chem.*
1078 *Phys. Discuss.*, 3(2), 1777–1804, doi:10.5194/acpd-3-1777-2003, 2003.

1079 Zhang, L., Vet, R., O'Brien, J. M., Mihele, C., Liang, Z. and Wiebe, A.: Dry deposition of individual nitrogen species at eight
1080 Canadian rural sites, *J. Geophys. Res. Atmos.*, doi:10.1029/2008JD010640, 2009.

1081 Zhang, L., Jacob, D. J., Liu, X., Logan, J. A., Chance, K., Eldering, A. and Bojkov, B. R.: Intercomparison methods for satellite
1082 measurements of atmospheric composition: Application to tropospheric ozone from TES and OMI, *Atmos. Chem. Phys.*,
1083 10(10), 4725–4739, doi:10.5194/acp-10-4725-2010, 2010.

1084 Zhang, L., Jacob, D. J., Knipping, E. M., Kumar, N., Munger, J. W., Carouge, C. C., Van Donkelaar, A., Wang, Y. X. and
1085 Chen, D.: Nitrogen deposition to the United States: Distribution, sources, and processes, *Atmos. Chem. Phys.*,
1086 doi:10.5194/acp-12-4539-2012, 2012.

1087 Zhou, P., Ganzeveld, L., Rannik, U., Zhou, L., Gierens, R., Taipale, D., Mammarella, I. and Boy, M.: Simulating ozone dry
1088 deposition at a boreal forest with a multi-layer canopy deposition model, *Atmos. Chem. Phys.*, 17(2), 1361–1379,
1089 doi:10.5194/acp-17-1361-2017, 2017.

1090 Zhou, S. S., Tai, A. P. K., Sun, S., Sadiq, M., Heald, C. L. and Geddes, J. A.: Coupling between surface ozone and leaf area

1091 index in a chemical transport model: Strength of feedback and implications for ozone air quality and vegetation health, *Atmos.*
1092 *Chem. Phys.*, doi:10.5194/acp-18-14133-2018, 2018.

1093 Zhu, Z., Bi, J., Pan, Y., Ganguly, S., Anav, A., Xu, L., Samanta, A., Piao, S., Nemani, R. R. and Myneni, R. B.: Global data
1094 sets of vegetation leaf area index (LAI)_{3g} and fraction of photosynthetically active radiation (FPAR)_{3g} derived from global
1095 inventory modeling and mapping studies (GIMMS) normalized difference vegetation index (NDVI_{3G}) for the period 1981 to
1096 2, *Remote Sens.*, doi:10.3390/rs5020927, 2013.

1097 Zhu, Z., Piao, S., Myneni, R. B., Huang, M., Zeng, Z., Canadell, J. G., Ciais, P., Sitch, S., Friedlingstein, P., Arneth, A., Cao,
1098 C., Cheng, L., Kato, E., Koven, C., Li, Y., Lian, X., Liu, Y., Liu, R., Mao, J., Pan, Y., Peng, S., Peñuelas, J., Poulter, B., Pugh,
1099 T. A. M., Stocker, B. D., Viovy, N., Wang, X., Wang, Y., Xiao, Z., Yang, H., Zaehle, S. and Zeng, N.: Greening of the Earth
1100 and its drivers, *Nat. Clim. Chang.*, 6(8), 791–795, doi:10.1038/nclimate3004, 2016.

1101